Ion distribution models for defect fluorite $ZrO_2 - AO_{1.5}$ (A = *Ln*, Y) solid solutions: I. Relationship between lattice parameter and composition

A.A. Bukaemskiy[a], V.L. Vinograd[a,b†,] P.M. Kowalski[b,c]

[a] *Institute of Energy and Climate Research (IEK-6), Nuclear Waste Management and Reactor Safety, Forschungszentrum Jülich, Jülich, Germany.*

[b] *JARA High Performance Computing, Schinkelstrasse 2, 52062 Aachen, Germany*

[c] *Institute of Energy and Climate Research (IEK-13): Theory and Computation of Energy Materials*

Received; accepted

Abstract

The composition dependence of the lattice constant, a, in $A_xB_{1-x}O_{2-0.5x}V_{0.5x}$, fluorite-type solid solutions (B = Zr, A = {Nd-Yb, Y}, V = oxygen vacancy) is characterized by changes in slope at $x \sim 1/3$, which cannot be described by existing models. Moreover, over the range of $0.15 \le x \le 1/3$ the a vs. x data on all systems can be fitted with a linear equation, $a = q + rx$, with the same intercept, q, however, over the range of $1/3 \le x \le 1/2$ the data bifurcate requiring different intercepts for A={Nd-Gd] and for A={Dy-Yb,Y} systems, implying steeper slopes for the first group. An adequate description is achieved via close-packing models involving two anion species, O^{2-} and V, and three combinations of cation species, namely ^{8}A, ^{7}B, ^{8}B ($0 \le x \le 1/3$), ^{7}A, ^{8}A, ^{7}B ($1/3 \le x \le 1/2$) and ^{8}A, ^{6}B, ^{7}B ($1/3 \le x \le 1/2$), that take into an account the constraint on the average coordination number, $K(x)$, of $K(x) = 8 - 2x$ and two additional short-range order (SRO) constrains referring to vacancy-vacancy avoidance and vacancy-to-Zr association. The consistent fit to a vs. x data with these models requires the effective size of the oxygen vacancy to be larger than the radius of the oxygen anion by ~11%. The latter observation seems to play an important role in the understanding of structure-property relationships in $A_xB_{1-x}O_{2-0.5x}V_{0.5x}$ systems.

Keywords: Defect fluorite, pyrochlore, solid solutions, structure-property relationship, short range order

1. Introduction

Besides diverse applications ranging from thermal barrier coating [1,2] to catalysts and catalyst washcoats [3], the zirconia based yttria and lanthanide doped fluorite- and pyrochlore-type ceramics were widely investigated as fast ionic conductors for solid oxide fuel cells [4-6] and oxygen sensors [7]. Over the last two decades the same materials attract attention as matrices for the immobilization of radionuclides [8-10]. Within the latter field of research the particular interest is in finding compounds

that are resistant to the radiation-induced self-amorphization. In ordered pyrochlore $A_2B_2O_7$ compounds (A={La, Nd, Sm, Eu, Gd, Y, Yb}) both the ionic conductivity and the resistance to self-irradiation correlate with the ratio of ionic radii of ^{8}A and ^{6}B cations, R_A/R_B [8, 11] suggesting that knowledge gained in electrochemical studies could appear useful in studies of waste management. In these systems, the ionic conductivity increases with the decrease in R_A/R_B such that the maximum is achieved at $R_A/R_B \sim$ 1.48, i.e. for $Eu_2Zr_2O_7$ [11]. On the other hand, the critical amorphization temperatures of $A_2Zr_2O_7$ and $A_2(Ti_{1-x}Zr_x)_2O_7$ pyrochlores decrease with the R_A/R_B ratio [8,12,13], while the condition of $R_A/R_B < 1.50$ defines a group of $A_2B_2O_7$ compounds characterized by not measurably low critical amorphization temperatures. These compounds cannot be converted under high-energy ion beam irradiation into amorphous state even at a room temperature. It is also well established that the R_A/R_B ratio of ~1.46 defines the stability limit of the pyrochlore structure. $A_2B_2O_7$ compounds with $R_A/R_B < 1.46$ crystallize in the disordered defect fluorite (DF, $Fm\bar{3}m$) structure, while those with $R_A/R_B > 1.46$ in the ordered pyrochlore (P, $Fd\bar{3}m$) structure [14, 15]. Thus, the maximum of ionic conductivity in $A_2Zr_2O_7$ systems occurs just above the DF/P boundary within the pyrochlore field [11], while a high radiation stability is relevant for compounds that fall into the fluorite field and for pyrochlores that have a high propensity to disorder, e.g. for $Gd_2Zr_2O_7$, with $R_A/R_B \sim 1.46$ [8,16]. Consistently with these observations, a strong correlation between ionic conductivity and degree of disorder was revealed in the electrochemical study of $Gd_2(Zr_xTi_{1-x})_2O_7$ system [17]. A four orders of a magnitude increase in the ionic conductivity with the increase in the mole fraction of Zr in the range of $0.2 < x < 1$ (i.e. decrease in R_A/R_B) was linked to the progressive disordering of both cationic and anionic sublattices of the pyrochlore structure [18].

In $A_xZr_{1-x}O_{2-0.5x}$ solid solutions distinct changes in ionic conductivity vs. composition occur at $x \sim 1/3$ and at $x \sim 1/2$ [14, 19]. Particularly, in the $Gd_xZr_{1-x}O_{2-0.5x}$ system at 800 °C the ionic conductivity increases with x reaching a maximum at $x \sim 0.18$, then falls down to the composition of $x \sim 1/3$, and then steadily increases reaching the second maximum at the composition of $x = 1/2$ [14, 19]. The fitting of the

conductivity data to the Arrhenius equation revealed distinct breaks in the composition dependence of the activation energy at $x \sim 1/3$ and $x \sim 1/2$ [14]. In $Nd_xZr_{1-x}O_{2-0.5x}$ and $Gd_xZr_{1-x}O_{2-0.5x}$ systems such breaks correlate with changes in the composition dependence of the *a* parameter of the fluorite lattice on *x* [14, 19]. Distinct changes in *a* vs. *x* slope occur in the both systems at the composition of $x \sim 1/3$. While in the $Nd_xZr_{1-x}O_{2-0.5x}$ system the change at $x \sim 1/3$ coincides with the appearance of pyrochlore-type superlattice reflections in X-ray diffraction patterns, it is not so in $Zr_{1-x}Gd_xO_{2-0.5x}$ system, where sharp P-type reflections appear only within the range of $0.45 < x < 0.62$ [19, 20]. Remarkably, the break in *a* vs. *x* slope at $x \sim 1/3$ also occurs in systems with A = {Dy-Yb, Y} [21-26], in which pyrochlore is not stable. These observations lead to the proposition that the wending point at $x \sim 1/3$ may not be necessarily related to the pyrochlore-type ordering, also reflecting changes in schemes of short-range order. Based on the EXAFS Zr-edge spectroscopy study Uehara et al. [27] suggested that the minimum in the ionic conductivity at $x \sim 1/3$ in $Gd_xZr_{1-x}O_{2-0.5x}$ system and the corresponding break in *a* vs. *x* slope reflects a type of short-range ordering, in which all Zr cations are bound to vacancies.

Short-range ordering in defect fluorite has been discussed as a plausible cause of the decrease in the ionic conductivity of $AO_{1.5}$ doped ZrO_2 solid solutions towards $x \sim 1/3$ [28]. Ab initio calculations coupled with molecular dynamics and kinetic Monte Carlo simulations [28-35] revealed that heights of activation energy barriers for vacancy/oxygen swaps in yttria stabilized zirconia (YSZ) strongly vary depending on the nature of cations and anions surrounding the vacancy-oxygen pair experiencing a swap. It has been shown that both cation-anion and anion-anion short-range interactions are responsible for this variation [31-35]. SRO has been also discussed as the cause of negative enthalpies of mixing measured calorimetrically in $A_xB_{1-x}O_{2-0.5x}$ systems A = {Sm, Gd, Dy, Y, Yb}, B ={Zr, Hf}[36-39]. Recently, renewed interest in SRO has been caused by application of pair distribution function (PDF) analysis of neutron total scattering data. The data on defect fluorite samples, such as $Ho_2Zr_2O_7$ and $Nd_xZr_{1-x}O_{2-0.5x}$ ($x = 0.27$), were fitted well with weberite structure model [40], suggesting a high degree of order remaining in defect fluorite above the order/disorder transition temperature. A weberite-type

model was also used to fit thermochemical data on the order/disorder transition in $Nd_xZr_{1-x}O_{2-0.5x}$ solid solution [41]. DFT calculations of the enthalpy of P/DF transition [41, 42] have shown that for Hf- and Zr-based $A_2B_2O_7$ systems weberite model performs significantly better in fitting solution calorimetry data [43, 44] than a quazi-random structure of defect fluorite. Valuable insights into the nature of local ordering in fluorite were obtained through atomistic simulations of $Y_xZr_{1-x}O_{2-0.5x}$ and $Sc_xZr_{1-x}O_{2-0.5x}$ systems based on the cluster expansion method [35, 45, 46]. These studies have shown that the cation and anion distributions are governed by two SRO principles, 1) the electrostatic energy driven vacancy-vacancy avoidance and 2) the strain energy driven association of a vacancy to the smaller cation (Zr). It has been also shown that the latter tendency is reverted when the sizes of A and B cation become comparable, as occurs, for example, in $Ln_2Th_2O_7$ compounds [47]. This has been attributed to a compromise between the short-range strain-driven association of V to B and the more long-range electrostatic association of V to A. Consequently, vacancies prefer to be second neighbours to A cations [33, 35, 46]. Long-range ordered structures, such as pyrochlore (x = 0.5) and delta phase (x = 4/7), as well as the theoretically predicted in the ZrO_2-Y_2O_3 system ground state structure with *C2/m* symmetry (x = 1/3) [48] follow the same principles. For example, in the *C2/m* structure vacancies reside at the 6-th nearest anion-anion distance, all Zr cations have one vacancy within their nearest anion configuration, while Y is at the second-neighbour distance to a vacancy. Strict following these principles implies that the set of accessible cation coordination numbers in fluorite solid solution could take the values of 6, 7, and 8 only, while in cases of $R_A >> R_B$ the average coordination number of A cations is always larger than this of B cations. Such a reduced spectrum of coordination environments is indeed confirmed in a number of spectroscopic and structural studies [49-53].

Atomistic simulation [16, 28, 54-67] and thermodynamic modelling studies guided by ab initio calculations [68] were instrumental in the understanding of the correlation between physical properties and the propensity pyrochlore ($x \sim 0.5$) compounds to disorder. The propensity to disorder of pyrochlore compounds was linked to low formation energies of cation anti-site and anion Frenkel defects. The low

energy of anion Frenkel pairs was shown to be the prerequisite of high concentration of vacancies within the 48f-oxygen sublattice in some of compounds and of their enhanced conductivity [54-56, 58, 59, 67], while the resistance to radiation damage was linked to a low rate of strain energy accumulation caused by low formation energies of cation anti-sites, anion Frenkel pairs or cation anti-sites coupled with anion Frenkel pairs [16, 60, 62, 66, 67].

On the other hand, the absence of a clear understanding of the breaks in structure/property relationships at $x \sim 1/3$ calls for a deeper analysis of short- and long-range order phenomena in non-stoichiometric defect fluorite. A general model allowing for structure/property correlation studies over the whole composition range of defect fluorite solid solutions is still to be developed. As changes in the ionic conductivity correlate with breaks in the slope of a vs. x dependencies, a comprehensive model, first of all, must accurately describe the data and provide a structural explanation of the breaks at $x \sim 1/3$ and $x \sim 1/2$. These fine features in a vs. x dependences in fluorite $A_xB_{1-x}O_{2-05.x}$ solid solutions are ignored in the majority of available models [69-75]. The present study, which is further referred as Part I, together with the Part II [76] aims at developing improved ion-distribution models of fluorite and pyrochlore solid solutions that allow an accurate description of a vs. x relationships via a detailed analysis of changes in cation coordination numbers. The present analysis is mostly focused on a vs. x data that presumably correspond to samples synthesized within 1673 – 1873 K interval. Thus, the temperature is ignored as a factor of the lattice parameter change. Part II [76] specifically considers the effect of the temperature on the lattice parameter. A more detailed understanding of structure/property relationships gained in the process of the model construction provides hints to the understanding of structural factors determining variations in the radiation stability and ionic conductivity in fluorite and pyrochlore compounds.

2. Models and Methods

This chapter is split into several sections. The first paragraph describes experimental *a* vs. *x* data ($0.15 < x \leq 0.5$) for $ZrO_2 - AO_{1.5}$ systems, A = {Nd-Yb, Y}, and presents their linear regression analysis. This analysis reveals three groups of the data, which are characterized by common ($x = 0$) intercepts and by significantly different *a* vs. *x* slopes. The second section describes previous models of *a* vs. *x* relationship illustrating their inability in reflecting the changes of slopes in the *a* vs. *x* data. The following third section provides equations, based on the ion-packing principle and on SRO constraints, which explain the observed differences in the linear behaviour within the three groups of data. The fourth paragraph develops a fitting strategy with which the parameters of these models, such as the effective size of a vacancy and the effective radii of 7-fold coordinated cations, are sequentially determined. The last paragraph describes methodical aspects of an independent approach of estimating the effective size of the vacancy based on *ab initio* simulations of pyrochlore supercell structures.

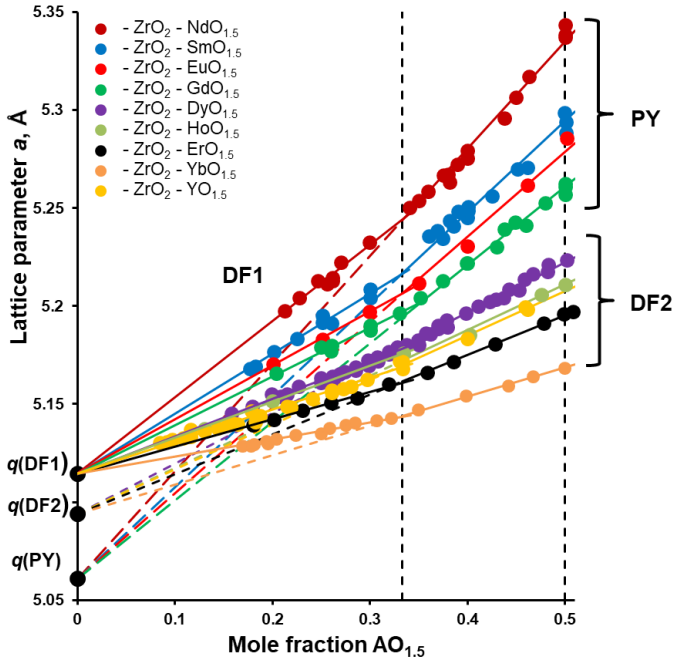

Figure 1. Experimental data on *a* vs. *x* behaviour in ZrO_2-$AO_{1.5}$ systems, (A={*Ln*,Y}): Nd [14, 41, 77, 78]; Sm [78-81]; Eu [82]; Gd [14, 19, 77, 78, 83]; Dy [21]; Ho [22]; Er [21]; Yb [21]; Y [23-26]. The lines are linear fits to the data constrained to pass through three different intercepts. Uncertainties in the original data are smaller than the size of the circles.

2.1. Processing of a vs. x data

Selected experimental data on the composition dependence of the lattice parameter in $ZrO_2 – AO_{1.5}$ (A = Nd-Yb, Y) fluorite- and pyrochlore-type solid solutions in the $0.15 < x \leq 0.5$ interval are plotted in Fig. 1. Pyrochlore superlattice reflections were reported in the systems of Nd – Gd. Visual analysis of the data on these systems shows a change in the slope in *a* vs. *x* dependencies at $x \sim 1/3$. In $ZrO_2 – NdO_{1.5}$ system pyrochlore reflections occur in the interval of $0.33 < x < 0.65$ [41], thus, the break at $x \sim 1/3$ can be logically associated with the fluorite/pyrochlore transition. In $ZrO_2 – GdO_{1.5}$ system P-type reflections occur only at $x > 0.45$ [28], however, the data within the interval of $0.33 \leq x \leq 0.5$ seem to fall on the same trend that is consistent with the data on the other systems with P-type reflections. Importantly, the data on Dy-Yb and Y-systems, where the P-type ordering is absent, also show similar, but slightly less prominent changes in the slope at the composition $x \sim 1/3$. Thus the whole set of $ZrO_2 – AO_{1.5}$ data splits into three groups. The first group includes data points for all systems that fall into the interval of $0.15 < x \leq 1/3$, the second and third groups include the data on pyrochlore-type (Nd-Gd) and fluorite-type (Dy-Yb, Y) systems, respectively, that fall into the interval of $1/3 \leq x \leq 1/2$. These groups will be further associated to different models of SRO/LRO.

Table 1.

Linear regression of *a* vs. *x* data.

System	*Interval*	*q*	*r*	*x**	*q*	*r*	*x**
$NdO_{1.5} – ZrO_2$	0 – 1/3	5.1142	0.3907	0.352	5.1145	0.3894	0.337
	1/3 - 1/2	5.0483	0.5781		5.0610	0.5481	
$SmO_{1.5} –ZrO_2$	0 – 1/3	5.1141	0.3078	0.300	5.1145	0.3062	0.332
	1/3 - 1/2	5.0787	0.4259		5.0610	0.4674	
$EuO_{1.5} – ZrO_2$	0 – 1/3	5.1165	0.2681	0.352	5.1145	0.2758	0.334
	1/3 - 1/2	5.0453	0.4702		5.0610	0.4358	
$GdO_{1.5} – ZrO_2$	0 – 1/3	5.1172	0.2394	0.333	5.1145	0.2490	0.354
	1/3 - 1/2	5.0717	0.3762		5.0610	0.4003	
$DyO_{1.5} – ZrO_2$	0 – 1/3	5.1151	0.1891	0.331	5.1145	0.1914	0.313
	1/3 - 1/2	5.0877	0.2720		5.0940	0.2569	

$ErO_{1.5} – ZrO_2$	0 – 1/3	5.1123	0.1486	0.352	5.1141	0.1394	0.324
	1/3 - 1/2	5.0904	0.2109		5.0940	0.2028	
$YbO_{1.5} – ZrO_2$	0 – 1/3	5.1111	0.1015	0.335	5.1145	0.0872	0.328
	1/3 - 1/2	5.0977	0.1415		5.0940	0.1498	
$YO_{1.5} – ZrO_2$	0 – 1/3	5.1151	0.1606	0.320	5.1145	0.1634	0.323
	1/3 - 1/2	5.0933	0.2287		5.0940	0.2270	

Note: x^* denotes the composition at which two linear equations intersect. The data for each system were fitted twice, in the [0, 1/3] and [1/3, 1/2] intervals. R^2 parameters were found to be in the range of 0.98 - 0.985 for all data sets.

Table 1 shows the results of the linear regression analysis of the experimental data shown in Fig. 1 under the assumption that the data on each chemical system falling in the intervals $0.15 < x \leq 1/3$ and $1/3 \leq x \leq 1/2$ can be fitted with two dissimilar linear equations of the type $a = q + rx$. Two variants of the fitting exercises were performed. The first (unconstrained) fit assumes that the q parameters in all chemical systems are independent of each other. The results are given in the columns 3-5. Column 5 lists the point of intersection, x^*, of the two linear equations. The second exercise explores the observation that the intercepts ($x = 0$) within each of the three groups vary insignificantly (q(DF1) = 5.115 ± 0.002 Å, q(PY) = 5.06 ± 0.02 Å, q(DF2) = 5.094 ± 0.004 Å) and restricts the q parameter to be the same within each of the three groups. The results of the second exercise are given in columns 6-8 of Table 1. An interesting observation is that the intersection point, x^*, (the second fitting exercise) appears to be very close to 1/3 (0.33±0.01), while this composition appears to be the same for DF1/PY and DF1/ DF2 intersections. The linear equations derived with the constrained fit are shown as lines in Fig. 1. The existence of the three dissimilar linear relationships in the $0.15 < x \leq 1/2$ interval constitute the main experimental observation which is addressed in our modelling study.

2.2. Previous models of a vs. x relationship

There have been many attempts of developing a general model of a vs. x dependence in $B_{1-x}A_xO_{2-0.5x}$ materials [69-75, 84, 85]. The research was mostly aimed at finding BO_2 - $AO_{1.5}$ systems approaching zero a vs. x slope. Such systems were thought to be favorable for fast ionic conductivity and for thermal barrier coating applications. Typically, the compositions of $x \leq 0.3$ were of concern. Models of Alexandrov et al. [69] and of Ingel and Lewis [70] were based on ion close-packing idea and on the assumption that the oxygen vacancy has the same size as the oxygen anion. In the study of Glushkova et al. [71] the effect of vacancies onto the cell volume was taken into account by defining the effective ionic radius of the average anion as a nonlinear function of x constrained with the condition that vacancies contribute zero volume effect. Kim [74] obtained equations for the compositional dependence of a in BO_2 - $AO_{1.5}$ and BO_2 - AO systems, B={Th, Ce, Zr, Hf}, A={*Ln*, Y, Sc, Sr, Ca, Mg} with linear regression assuming compliance with Vegard's law and adopting Shannon's values of cation radii [86]. The total effect on the a parameter due to a dopant addition was split into a positive contribution proportional to the difference of ionic radii of A and B cations in the 8-fold coordination and a negative contribution proportional to the difference in formal charges of these cations. Hong and Virkar [75] developed a model based on the ion-packing concept, which formally complied with the two-parameter equation of Kim [74] and with a linearized version of Glushkova's model [68]. The model of Hong and Virkar [75] related the a parameter to the sum of ionic radii of cations and anions, $\langle R_c \rangle$ and $\langle R_a \rangle$,

$$a = \frac{4}{\sqrt{3}}\left(\langle R_c \rangle + \langle R_a \rangle\right). \quad (1)$$

Eqn. 1 assumes that cations and anions touch themselves along the body diagonal of a cubic cluster built by centres of 8 nearest anions. The cation radius is written as the average of ionic radii of A and B cations, R_A and R_B,

$$\langle R_c \rangle = (1-x) R_A + x R_B. \quad (2)$$

Similarly, the average radius of the anion is built of the contributions from the oxygen anion and the vacancy, which for III-valent dopants give

$$\langle R_a \rangle = \frac{2-0.5x}{2} R_O + \frac{0.5x}{2} R_V, \quad (3)$$

where R_O and R_V are the radii of an oxygen anion and of a vacancy, respectively. Under the assumption that both A and B cations adopt the 8-fold coordination, the a vs. x dependence in a $A_xB_{1-x}O_{2-0.5x}$ solid solution is given by the following linear equation [75]

$$a = \frac{4}{\sqrt{3}}\left(R_B^8 + R_O\right) + x\frac{4}{\sqrt{3}}¿. \quad (4)$$

The only unknown parameter in this model is the vacancy radius. Many studies attempted finding this parameter through fitting experimental a vs. x data [75, 87, 88]. The general conclusion was that a replacement of a B^{+4} cation by an A^{+3} cation causes a dilation, while the vacancy addition causes a contraction. The effective size of the vacancy appeared to be significantly *smaller* than the ionic radius of the oxygen atom. Although the latter result is justified by an accurate fit to the structural data at low dopant levels [75, 87, 88], it contradicts to the intuitive presumption that cations adjacent to a vacant site should be pushed away due to the loss of the attracting negative charge, thus giving a larger space to the vacancy. Such a shift in the position of the nearest cations is indeed seen in atomistically simulated structures [87, 88]. The simulations show also that the anions move towards the vacancy, thus causing a contraction effect. These observations suggest that both the dilation and contraction effects are absorbed by the model of Hong and Virkar [75] resulting in the effectively smaller size of the vacancy. Although such a description is legitimate, the model [75] becomes progressively less accurate when the composition approaches the $AO_{1.5}$ end-member (Fig. 2). The problem can be traced down to the intrinsic assumption [75] that both A and B cations remain 8-fold over the whole composition domain of $0 \le x \le$

1. Certainly, such an assumption becomes inaccurate at $x \sim 1$, where the average coordination number of A cations is 6.

Nakamura [84, 85] proposed a series of models that explicitly took into an account the change in the average cation coordination number, $K(x)$, with the composition

$$K(x)=8-2x, \tag{5}$$

that occurs due to the addition of vacancies. Nakamura [84] defined a radius functional of a cation, $r\left[K(x)\right]$, and obtained an interpolation equation for a vs. x that passed exactly through the lattice parameters of BO_2 and $AO_{1.5}$ end-members (B = {Hf, Zr, Ce, Th}, A = *Ln*). Differently from the model of Hong and Virkar [75], the model of Nakamura [84] predicted a non-linear dependence between a and x, providing a better description to the data over the whole composition interval (Fig. 2). This approach has been then extended to a series of improved "non-random" models, which took into account association effects between vacancies and cations [84, 85]. Importantly, the mapping of these models onto the ion packing model suggested that the effective size of a vacancy is larger than the radius of the oxygen anion [84]. Eqn. 5 was also employed by Yashima et al. [72, 73] within an ion-packing approach. Several models were developed that took into an account different modes of vacancy association to cations A and B. Particularly, the "model 2" [72] considered a case, in which all vacancies occur within clusters of four B cations, such that A cations are always 8-fold coordinated, while B cations could be in 8- and 7-fold coordination depending on the composition and on the constraint of Eqn. 5. The effective radius of the vacancy was assumed equal to the ionic radius of O^2. Fitting this model to a vs. x data on $ZrO_2 - AO_{1.5}$ systems showed a consistent deviation between the predicted and measured a vs. x slopes. Below we will show that the removing of the unnecessary constraint of $R_V = R_O$ from Yashima's model 2 or, otherwise, the including of the constraint of Eqn. 5 into the model of Hong and Virkar [75] provides a drastic improvement in fitting of a vs. x data.

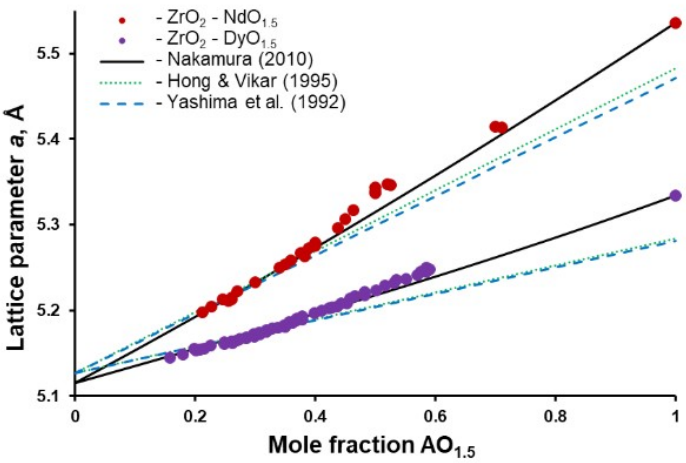

Fig. 2. Selected experimental *a* vs. *x* data for ZrO_2-*Ln*$O_{1.5}$ systems in comparison with theoretical model predictions. Both linear models of Yashima et al. [72] (model 2), Hong and Virkar [75] and non-linear interpolation model of Nakamura [84] fail to predict changes of slope in the data occurring at intermediate compositions. The experimental data are from the same sources as in Fig. 1.

2.3. Models of a vs. x relationship consistent with SRO

In the following derivations different types of SRO are introduced as rigid constraints/postulates. The thermodynamic validity of these postulates is justified by a successful modelling of *a* vs. *x* data (see the Results section) and by thermodynamic modelling that is presented separately in Part II [76]. The most important postulate that is applicable to all models is the requirement that the coordination number of any cation cannot be smaller than six. We interpret this constraint as a consequence of the vacancy-vacancy avoidance principle that forbids vacancies to approach each other closer than the third-nearest neighbour (3NN) distance. This postulate will be further referred to as "weak VV avoidance" (wVVA). It is assumed to be valid over $0 \leq x \leq 1$. Within the domain of $0 \leq x \leq 1/2$ another rule can be set that forbids the vacancies to approach each other closer than 4NN. This more rigid constraint is equivalent to the request that the coordination number of any cation is larger than six. A cation and anion distribution that satisfies such a rigid avoidance constraint will be referred to as rVVA. We also assume that within the domain of $1/2 \leq x \leq 1$ the weak VVA is combined with a different avoidance principle that affects oxygen anions. This principle dictates the coordination number of any cation to be smaller than eight.

This constraint is referred here as rOOA (rigid oxygen-oxygen avoidance). rOOA forbids extra oxygen anions that need to be inserted into an ordered vacancy sublattice of the $AO_{1.5}$ endmember to be at 3NN anion-anion distances of each other. This excludes a possibility for a cation to be 8-fold coordinated. wOOA is equivalent to wVVA (see the Supplementary Information file for a detailed discussion of OOA). The applicability of either VVA or OOA principles splits the model space into $0 \le x \le 1/2$ and $1/2 \le x \le 1$ domains. Another important dimension within the ordering space is the degree of vacancy-to-cation association. The tendency to vacancy-to-B-cation association (VBA) implies that the coordination of A cations is always larger than that of B cations and that this difference is maximized. The realization of this principle depends on the composition and on the degree of VVA. Within the $0 \le x \le 1/2$ domain VBA can be fulfilled in two variants. Rigid VBA (rVBA) requires the coordination number of A cations to be always eight, i.e. $[^7A] = 0$ and $[^6A] = 0$ ("no vacancy in the neighbourhood of A"). When this request cannot be fulfilled due a composition constraint, a less rigid principle (wVBA) ("at least one vacancy is in the neighbourhood of each B", i.e. $[^8B] = 0$) is maintained instead. Within the $1/2 \le x \le 1$ domain VBA can be reformulated as oxygen-to-A-cation association principle (OAA), which also exists in two variants. Rigid OAA (rOAA) requests B cations to be always 6-fold coordinated. The less rigid variant (wOAA) requests $[^6A] = 0$ ("at least one extra O anion is in the close neighbourhood of each A"). Further, we note that a combination of rVVA and rVBA or a combination rOOA and rOAA is possible only in limited composition domains. When these constraints cannot be simultaneously satisfied, one of them is released to its less rigid variant. Combining VVA with VBA and OOA with OAA constraints according to the scheme of Table 2 gives rise to six models. A detailed derivation of these models is given in Supplementary Information file. A short, but essential, derivation of models DF1, DF2 and PY relevant for the $0 \le x \le 1/2$ domain is outlined below.

Table 2

Types of SRO restrictions satisfied in models of SRO

Model: x-range	VVA	VBA	OOA	OAA

DF1: [0,1/3]	rigid	rigid		
DF2: [1/3, 1/2]	rigid	weak		
PY: [1/3, 1/2]	weak	rigid		
PYM: [1/2, 2/3]			weak	rigid
DF2M: [1/2, 2/3]			rigid	weak
DF1M: [2/3, 1]			rigid	rigid

Notes: VVA – vacancy-vacancy avoidance; VBA – vacancy-B-cation association; OOA – oxygen-oxygen avoidance; OAA – oxygen-A-cation association.

The cation fractions of any model must satisfy the general constraint on the average coordination number

$$K(x)=8¿, \qquad (6)$$

where $K(x) = 8 – 2x$.

The compliance with rVVA implies $[^6A] = 0$ and $[^6B] = 0$, while the compliance with rVBA implies $[^7A] = 0$ and $[^6A] = 0$. Eqn. 6 is then simplified to

$$K(x)(DF1)=8¿. \qquad (7)$$

The fractions of $[^8A]$, $[^8B]$ and $[^7B]$ are further worked out noting that $[^8A] = x$, $[^8B] = (1-x)\,p_B^8$ and $[^7B] = (1-x)\,p_B^7$, where p_B^8 and p_B^7 have the meaning of conditional probabilities that satisfy $p_B^8 + p_B^7 = 1$. Together with Eqns. 5 and 7 this gives $[^8B]$ ¿ $1-3\,x$ and $[^7B]$ ¿ $2\,x$. The model that satisfies both rVVA and rVBA is further referred to as “DF1”. The corresponding solid solution is described with the formula $(^8B_{1-3x}{}^7B_{2x}{}^8A_x)O_{2-0.5x}$. The cation fractions are given in Table 3. Clearly, DF1 is defined only

within the interval of $0 \leq x \leq 1/3$. At the limiting composition of $x = 1/3$ ^{8}B-type cations vanish, implying that all B cations have one vacancy in their immediate neighbourhood.

It follows that within the domain of $1/3 \leq x \leq 1/2$ either VBA or VVA should be made less rigid. The first option of keeping the constraint of rVVA implies the necessity of increasing the fraction of [^{7}A], i.e. releasing the rVBA to wVBA. Employing the wVBA constraint of [^{8}B] `= 0, the condition on the average coordination number is then written

$$K(x)(DF2) = 8¿. \quad (8)$$

The fractions of [^{8}A], [^{7}B] and [^{7}A] can be worked out noting that [^{7}B] = $1 - x$, [^{8}A] ¿ xp_A^8 and [^{7}A] ¿ xp_A^7, where $p_A^8 + p_A^7 = 1$. Satisfying the constraints of Eqns. 5 and 8 gives [^{7}A] = $3x - 1$, [^{8}A] = $1 - 2x$ and [^{7}B] = $1 - x$. This model is further referred to as "DF2".

The second alternative over the domain of $1/3 \leq x \leq 1/2$ is to release rVVA to wVVA, while keeping rVBA. This implies that A cations are not allowed to be associated with vacancies, i.e. the constraints of [^{7}A] = 0 and [^{6}A] = 0 hold as in DF1, while B cations with 6-fold coordination are allowed to be formed. These conditions lead to the relationship

$$K(x)(PY) = 8¿, \quad (9)$$

which together with Eqn. 5 gives [^{8}A] = x, [^{6}B] = $3x - 1$ and [^{7}B] = $2 - 4x$. The solid solution has the structural formula of $(^{6}B_{3x-1}{}^{7}B_{2-4x}{}^{8}A_x)O_{2-0.5x}$. Note that at $x = 1/2$ this formula complies with $^{8}A_2{}^{6}B_2O_7$ pyrochlore. The cation fractions of all models are given in Table 3.

Table 3

Cation fractions in SRO models of fluorite

Model: x-range	^{8}B	^{7}B	^{6}B	^{8}A	^{7}A	^{6}A

DF1: [0,1/3]	$1 - 3x$	$2x$	0	x	0	0
DF2: [1/3, 1/2]	0	$1 - x$	0	$1 - 2x$	$3x - 1$	0
PY: [1/3, 1/2]	0	$2 - 4x$	$3x - 1$	x	0	0
PYM: [1/2, 2/3]	0	0	$1 - x$	$2 - 3x$	$4x - 2$	0
DF2M: [1/2, 2/3]	0	$2 - 3x$	$2x - 1$	0	x	0
DF1M: [2/3, 1]	0	0	$1 - x$	0	$2 - 2x$	$3x - 2$

Table 4

Models for a vs. x relationship in short-range ordered defect fluorite and pyrochlore solid solutions.

Model	q	r
DF1 : [0,1/3]	$\frac{4}{\sqrt{3}}\left(R_B^8 + R_O\right)$	$\frac{4}{\sqrt{3}}$¿
DF2 : [1/3, 1/2]	$\frac{4}{\sqrt{3}}\left(R_A^8 - R_A^7 + R_B^7 + R_O\right)$	$\frac{4}{\sqrt{3}}$¿
PY: [1/3, 1/2]	$\frac{4}{\sqrt{3}}\left(2R_B^7 - R_B^6 + R_O\right)$	$\frac{4}{\sqrt{3}}$¿
PYM : [1/2, 2/3]	$\frac{4}{\sqrt{3}}\left(2R_A^8 - 2R_A^7 + R_B^6 + R_O\right)$	$\frac{4}{\sqrt{3}}$¿
DF2M : [1/2, 2/3]	$\frac{4}{\sqrt{3}}\left(2R_B^7 - R_{B\square}^{6\square} + R_O\right)$	$\frac{4}{\sqrt{3}}$¿
DF1M : [2/3, 1]	$\frac{4}{\sqrt{3}}\left(2R_A^7 - 2R_A^6 + R_B^6 + R_O\right)$	$\frac{4}{\sqrt{3}}$¿

Note: Each model is defined by q and r values to be substituted into a linear equation of $a = q + rx$.

2.4. Determination of model parameters from a fit to a vs. x data

Table 3 permits computation of the average cation radii. Upon substituting the relevant cation fractions into Eqns. 2 and 1 and after a rearrangement linear relationships $a = q + rx$ between the lattice constant and the composition are obtained as given in Table 4. A logical assumption is that the first three equations, i.e. the models DF1, PY and DF2, can be put into the correspondence with the three groups of *a* vs. *x* data discussed above. The form of equations in Table 4 shows that the slopes and the intercepts can be predicted from tabulated Shannon's radii, under the conditions that the radii of 7-fold coordinated cations are refined and that the effective size of the vacancy is determined. These parameters are determined here along the following procedure:

1) determination of a refined value of R_O from the average intercept q of the first group of data using DF1 model,
2) determination of a refined value of R^7_{Zr} from the average intercept q of the second group of data using PY model,
3) determination of R_V from the slopes r of the first group of data using DF1 model,
4) refining values of R^7_A, A = {Dy-Yb, Y}, from slopes r of the third group of data using DF2 model and the value of R_V,
5) refining values of R^7_A, A = {Nd-Gd}, from slopes r of the second group of data using PYM model using the value of R_V,
6) determination of R_V for La and Pr from a values in pyrochlore compounds at $x = 0.5$ using PY model,
7) determination of the average value of R_V.

In this procedure the radii of cations in 6-fold and 8-fold coordination are adopted from Shannon [83].

2.5. Determination of the effective vacancy radius from ab initio simulations

The size of a vacancy relative to the size of an oxygen anion can be estimated with ab initio calculations by comparing volumes of Zr_4V and Zr_4O tetrahedrons formed about the 8b site in supercells derived from ordered $A_2Zr_2O_7$ pyrochlores. The supercell with a Zr_4O tetrahedron was made by transferring an O atom from a 48f site which is not a neighbour of the vacant 8a site. The volumes of the tetrahedrons were computed from relaxed positions of the four Zr atoms. The relative vacancy size was estimated with the equation

$$\frac{R_V}{R_O}=\frac{D_{V-Zr}-R_{Zr}^6}{D_{O-Zr}-R_{Zr}^7}, \quad (10)$$

where $D_{X\text{-}Zr}$ is the average distance from the centre of a tetrahedron, which is occupied by and anion, to its corner, which is occupied by Zr. The distance was computed as follows

$$D_{X-Zr}=\frac{\sqrt[2]{3}\sqrt[3]{3\,V_{tet}}}{2}, \quad (11)$$

where V_{tet} is the tetrahedron's volume. In these calculations we have used the already computed set of pyrochlore structures [66, 67]. These structures were computed using DFT Quantum-ESPRESSO code [89] with ultrasoft pseudopotentials [90] and PBE exchange-correlation functional [91].

3. Results

Here the fitting scheme outlined in the Methods section is applied to determining the model parameters. In this scheme the first group of data, i.e. all systems (A={Nd-Yb, Y}) within the range of $0.15 < x \leq 1/3$, is associated with the DF1 model, while the second and the third groups that include data on the systems of Nd-Gd and Dy-Yb, Y in the range of $1/3 \leq x \leq 1/2$, are associated with the models PY and DF2, respectively. We note that our original assumption that each group of data can be defined by a

common intercept has to be modified in the relation to the third group of data, as the mathematical expression defining the intercept in the model DF2 depends on $R_A^8 - R_A^7$ and thus cannot be regarded as a constant for all systems in this group. On the other hand, we note that the difference of the radii of ^{8}A and ^{7}A varies only slightly within the row of Dy-Yb and for Y. This explains the seemingly constant intercept within the third group of data. The cation radii resulting of the fitting exercise are given in Table 5. Other results are discussed in more detail below.

Table 5. The effective ionic radii used in the description of the experimental *a* vs. *x* data.

A	R_A^6	R_A^7	R_A^8	R_V
La	1.032	1.10 (1.10)	1.16	1.569
Pr	0.99	1.058 (1.058*)	1.126	1.530
Nd	0.938	1.043 (1.024*)	1.109	1.546
Sm	0.958	1.015 (1.02)	1.079	1.522
Eu	0.947	1.01 (1.01)	1.066	1.521
Gd	0.938	0.995 (1.00)	1.053	1.520
Dy	0.912	0.967 (0.97)	1.027	1.531
Ho	0.901	0.948 (0.958*)	1.015	1.565
Er	0.89	0.943 (0.945)	1.004	1.533
Yb	0.868	0.923 (0.925)	0.985	1.518
Y	0.9	0.957 (0.96)	1.019	1.514
B	R_B^6	R_B^7	R_B^8	R_O
Zr	0.72	0.7684 (0.78*)	0.84	1.375 (1.38)

Note: the values for 6- and 8-fold coordinated cations are from Shannon [86], the values for the 7-fold coordination are estimated here. The corresponding values for 7-fold coordinated cations from Shannon [86] are given in brackets. The values with * sign are the averages of the radii of 6-fold and 8-fold coordinated cations. The value of R_O is slightly modified from the value of Shannon [86]. The old value is given in brackets.

3.1. Sizes of the oxygen anion and of the vacancy

From the experimental value of the intercept of the first group of data q = 5.115±0.002 Å (Table 1) using the radius of ^{8}Zr of 0.84 Å from Shannon [86] we find R_O = 1.375±0.001Å, which is just a bit smaller than the tabulated value of 1.38 Å. We note that the refined value of R_O also compares well with the value of 1.378±0.004Å from an earlier study of Shannon and Prewitt [92]. We assume the presently derived value of 1.375 to be specifically applicable to Zr-based fluorite-type materials. From the common intercept of the second group of data q = 5.06±0.02 Å (Table 1) we find R^{7}_{Zr} = 0.768±0.003 Å, which differs from Shannon's value of 0.78. Using the r values for the first group of data (column 7 in Table 1) and the corresponding expression for r (model DF1, Table 4) we compute the effective radii of the vacancy. The obtained values for Nd – Yb systems are plotted in Fig. 3. The average R_V value of 1.53±0.02 Å significantly exceeds the ionic radius of the oxygen atom. The same figure shows R_V values computed with the model of Hong and Virkar [75] (Eqn. 4). The latter values are significantly smaller than the effective radius of O^{2-} falling in the range of 0.95-0.98 Å.

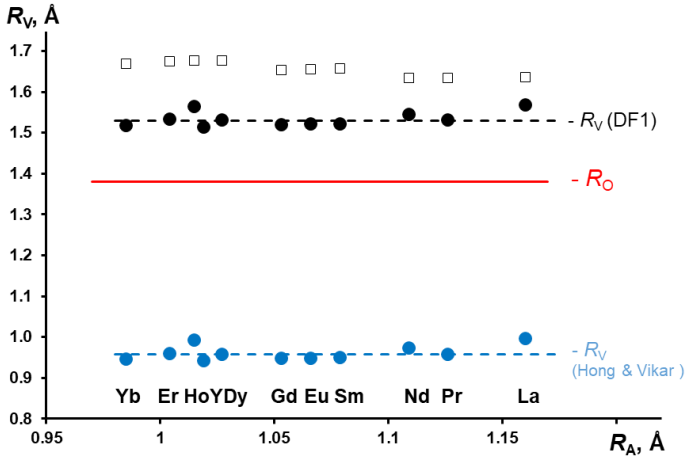

Figure 3. Effective vacancy sizes in ZrO_2 – $AO_{1.5}$ (A = *Ln*,Y) systems determined with the model DF1 (the upper set of solid circles) and with the model of Hong and Virkar [75] (the lower set of solid circles). The vacancy sizes in the cases of A = La and A = Pr are estimated from a values of pyrochlore compounds using model PY. Open squares show the results of the vacancy size estimation from DFT calculations.

The effective radii of O^{2-} and ^{7}Zr and the average values of the effective vacancy radii obtained via the fitting of DF1 and PY models to the first and second sets of the data were then set as constrains within the DF2 model and applied to the third group of data. This exercise allowed refining values of R_A^7 in systems of Dy-Yb and Y. These fitted values are compared to Shannon's data in Table 5. Similarly, R_A^7 values for the systems with A={Nd-Gd} were fitted with PYM model to the available data on pyrochlore-type compounds with the compositions of $0.5 \leq x \leq 0.77$. The fitted R_A^7 values are listed in Table 5. The data listed in Table 5 provide a complete set of constants needed for the description of all available *a* vs. *x* data on $ZrO_2 - AO_{1.5}$ systems, A={*Ln*, Y}. Fig. 4 compares *a* vs. *x* dependencies calculated with the models DF1, DF2, PY, PYM, DF2M and DF1M with the experimental data.

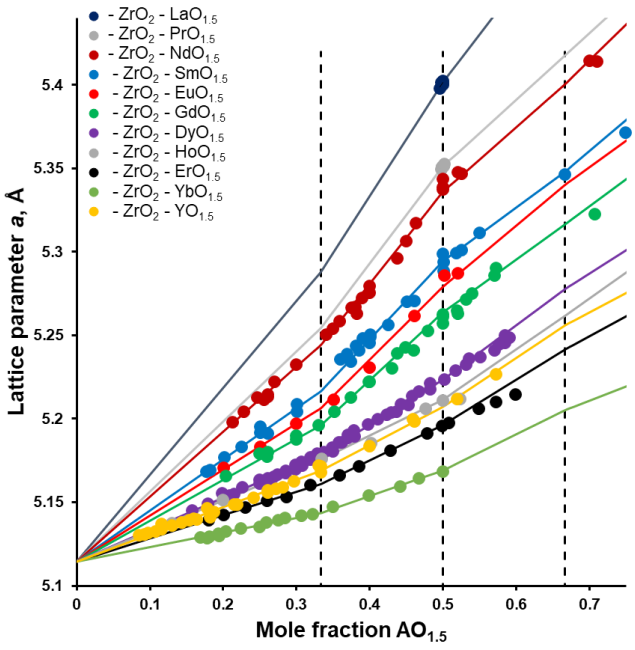

Fig. 4. Experimental data on the systems $ZrO_2 - AO_{1.5}$ systems, A={*Ln*, Y} described with the six models. The effective vacancy sizes for all systems, excluding Pr and La, were determined using the DF1 model applied to the data in the range of $0.15 < x < 0.33$. These sizes were further used in the other five models. The vacancy sizes in Pr and La systems were fitted by applying PY model to available experimental *a* vs. *x* data on Pr [93] and La [94] compounds.

3.2. Constraints to the vacancy size from atomistic simulations

The ab initio computed vacancy sizes vary in the range of 1.64-1.68 Å with a tendency of a slight increase along the lanthanide series of La-Yb (Fig. 3). The absolute values of R_V were estimated using R_O = 1.375±0.001Å. The radii of ^{6}Zr and ^{7}Zr are from Table 5. The larger values estimated ab initio may result from the application of the PBE exchange-correlation functional, which is known to overestimate volumes by a few percent [95]. Also, the rather small size of the supercell does allow to fully screen the effect of the removed vacancy onto the tetrahedron size. Nevertheless, the ab initio simulations show that the effective size of the oxygen vacancy is significantly larger than the ionic radius of the oxygen anion, consistently with the result obtained via the fitting of the DF1 model to the experimental data. Importantly, the simulations show that the vacancy radius does not depend significantly on the type of *Ln* consistently with the results of the fitting.

3.3. Testing the model against an extended set of a vs. x data

Ternary pyrochlore systems, e.g. $La_{2-y}Y_yZr_2O_7$ and $Ho_{2-y}Nd_yZr_2O_7$ [96, 97] are particularly interesting for testing the present model providing data on volume effects of DF/P transitions. Changing the *y* parameter in these systems allows crossing the DF/P boundary and measuring the associated change in the lattice parameter. The data on these and similar systems show that the lattice parameter changes abruptly at the order/disorder transition such that the volume of the disordered phase becomes significantly smaller. Here we hypothesize that the change in the lattice parameter can be attributed to the change from the ^{6}B + ^{8}A scheme of order to the ^{7}B + ^{7}A scheme. At x = 0.5 the PY and DF2 models comply with the equations

$$a(PY)=\frac{4}{\sqrt{3}}\left(0.5R_B^6+0.5R_A^8+0.875R_O+0.125R_V\right) \quad (12)$$

and

$$a(DF2)=\frac{4}{\sqrt{3}}\left(0.5R_B^7+0.5R_A^7+0.875R_O+0.125R_V\right), \quad (13)$$

respectively. These equations predict that the lattice parameters of stoichiometric $B_2A_2O_7$ compounds, A={*Ln*, Y}, with the pyrochlores and fluorite structure should depend linearly on R_A^8 and R_A^7, respectively, while the coefficient of proportionality is equal to the same value of $\frac{2}{\sqrt[3]{V}}$ 1.1574. Fig. 5 shows that this prediction is indeed fulfilled for pyrochlores and defect fluorites with the compositions of $x \sim 0.5$. Moreover, the data for the ternary $La_{2-y}Y_yZr_2O_7$ pyrochlores and fluorites [96] fall on the same two linear trends (Fig. 5, a), suggesting that the P/DF transition observed in this system can be indeed interpreted as the PY/DF2 transition (Fig. 5, b).

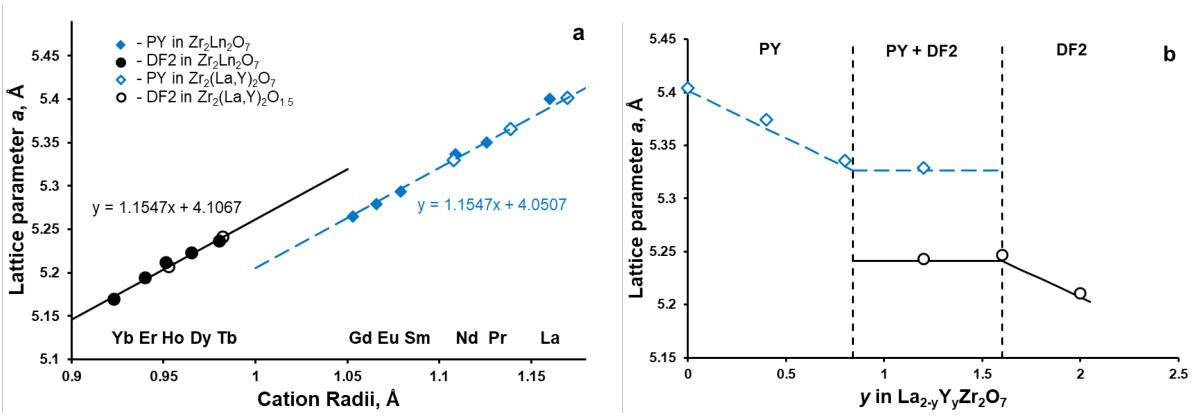

Fig. 5. Lattice parameters in $A_2Zr_2O_7$ compounds, A= {*Ln*, Y}, with pyrochlore and fluorite structures plotted as functions of A cation radii (a) and of composition (b). The experimental data for binary systems (solid circles) are from the same sources as in Figures 1 and 4. The solid and dashed lines in (a) correspond to Eqns. 12 and 13, respectively. The variation of the lattice parameter in (b) as a function of *y* is modelled by expressing R_A^8 or R_A^7 in Eqns. 12, 13 as linear combinations of R_{La}^8

and R_Y^8 or R_{La}^7 and R_Y^7, respectively. The data on the ternary $La_{2-y}Y_yZr_2O_7$ pyrochlores and fluorites (open circles) are from Whittle et al. [96].

4. Discussion

The effects of order on the lattice parameter are linked here to deviations of actual coordination numbers of A and B cations from the average coordination number given by the linear relationship $K = 8 - 2x$ (Fig. 6). The breaks in a vs. x relationships at $x \sim 1/3$, $x \sim 1/2$ and $x \sim 2/3$ are direct consequences of abrupt changes in the spectrum of coordination numbers. We argue here that other physical properties, such as variations in ionic conductivity and in radiation resistance, can be also associated with the changes in coordination numbers, and, thus, linked together within the same conceptual frame. An important prerequisite to the success of this description is the separation of the expansion effect imposed by a vacancy on its immediate cation neighbours from the total negative effect due the vacancy insertion on the lattice parameter. We begin the discussion with this important issue.

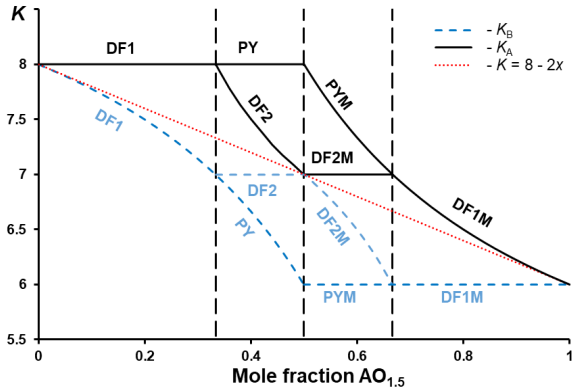

Fig. 6. Variation of the total average cation coordination number, K and of the average coordination numbers of A and B cations, K_A and K_B, as functions of the composition within the six models.

4.1. The effect of a vacancy insertion is split into extension and contraction effects.

The conclusion of $R_V > R_O$ formally contradicts the results of the previous studies [75, 87, 88], in which the lattice contraction due to a vacancy insertion (at low dopant levels) was described under the

assumption that the effective size of a vacancy is significantly smaller than the ionic radius of an oxygen anion. This contradiction is analysed here within a more complex model in which the total lattice contraction is split into an extension and a contraction effects. The latter contraction effect is attributed here to the change in coordination numbers of B cations due to the presence of vacancies. In the previous studies [75, 87, 88] the coordination numbers of all cations were fixed to be eight despite the presence of vacancies in the neighbourhood of certain cations.

Comparing the slope *r* defined by DF1 model (see the first row in Table 4) with the slope defined by Eqn. 4, i.e. in the model of Hong and Virkar [75], we find

$$R_V(this\ study) = R_V(Hong \wedge Virkar) + 8\left(R_B^8 - R_B^7\right). \quad (14)$$

This equation shows that the difference in the estimated vacancy sizes of ~0.573 Å obtained in the present and in the previous studies [75, 87, 88] (Fig. 3) is attributed to the change in the coordination number of eight B cations. This factor was not included in previous models. The difference in the effective sizes of the vacancy and the oxygen anion of 0.155±0.02 Å estimated here (R_V =1.53±0.02 Å, R_O =1.375±0.001 Å) is consistent with the relaxation pattern about an isolated vacancy [87, 88, 98] and about a divacancy [99] seen in ab initio calculations. For example, the calculations of Stapper et al. [98] on YSZ show that the four nearest Zr atoms move away from the vacancy along [111] by ~0.18 Å. On the other hand, the same calculations [98] show that the six nearest oxygen atoms move towards the vacancy along [100] by ~0.24 Å. As the closest Zr-(O,V) distance in fluorite is collinear with [111], the first effect can be easily simulated within ion-packing model by increasing the size of a vacancy. The second effect cannot be directly simulated within the ion-packing approach, because in this approach all ions must remain in their ideal positions of the fluorite structure. One possibility is to map both the dilation and the contraction effects onto the vacancy size [75, 87, 88]. We argue that a better option is to include the contraction effect into the average cation radius, linking its change to the change in the

coordination number of the cations nearest to the vacancy. Note that the shift of the oxygen anions towards the vacancy along [100] means simultaneously that these anions approach the four Zr cations more closely. The average change in the Zr-O distance can be thus absorbed by the smaller size of ^{7}Zr. Effectively, by relating the shrinkages of Zr-O distances to the difference in the radii of ^{7}Zr and ^{8}Zr, we map the contraction effect onto the [111] direction, where it can be separated into the contributions from cations and anions. The insertion of a vacancy causes four Zr-(O,V) bonds to expand along [111] by 0.155 Å, while the change in the coordination of four Zr cations from 8 to 7 causes the contraction of 32 bonds along the same direction by ~0.072 Å. Thus the effect of the change in the cation coordination on the length of a Zr-(O,V) bond has eight times larger weight than the change of the vacancy size. Thus, the contraction effect due to the change in coordination per vacancy is $8\left(R_B^7-R_B^8\right)$, consistently with Eqn. 14. The fitted value of R_{Zr}^7 of 0.7684 Å, which follows from our modelling scheme, appears to be very reasonable considering $R_{Zr}^6=0.72$, $R_{Zr}^8=0.84$ and $R_{Zr}^7=0.76$ from Shannon [86]. The latter value in [86] is apparently the average of the first two. The total effect due to a vacancy onto a Zr-(O,V) bond is negative (0.155 − 0.573 = −0.418 Å), consistently with the conclusion of [75, 87, 88].

We think that the present description that splits the vacancy effect into two contributions is more physical as it reflects the primary effect of the lattice accommodation to the vacancy, which is certainly the extension due to the loss of the negative charge of O^{2-}. It also reflects the contraction effect by accounting for the change in cation coordination. Importantly, the latter aspect provides more flexibility in fitting *a* vs. *x* data as it allows distinguishing between the effects due to 7- and 6-fold cations, i.e. the effects of DF1- and of pyrochlore-type ordering. Here we remind that the pyrochlore ordering implies the formation of 6-fold B cations about the vacancies, and this alone explains the different slopes of DF1 and PY models. This circumstance allows to use the same vacancy size in DF1 and PY models. The present DFT calculations based on the pyrochlore supercell show that the effective size of a vacancy in this structure is consistently larger than the ionic radius of the oxygen atom, being practically

independent on the Ln atom. This supports the present finding all *a* vs. *x* data can be modelled with a vacancy of a fixed radius, which is significantly larger than that of O^{2-}.

4.2. SRO and LRO in defect fluorite are driven by strain energy minimization due to the association of a large vacancy to the smaller cation.

The concept of a large vacancy appears useful in rationalizing forces that dive the ordering. The deviation of the coordination numbers from the average statistical value can formally be prescribed to reactions between cation species. Particularly, the occurrences of ^{7}A and ^{7}B cations in defect fluorite and of ^{6}B and ^{8}A in pyrochlore can be attributed to the reactions

$$^{8}B + {}^{6}A = {}^{7}B + {}^{7}A, \quad (15)$$

and

$$^{8}B + {}^{6}A = {}^{6}B + {}^{8}A, \quad (16)$$

The consistency of the present modelling scheme requires the reactions (15) and (16) to be strongly shifted to the right. The reaction progresses can be qualitatively understood by rewriting the same reactions in the form

$$O\text{-}{}^{8}B\text{-}O + V\text{-}{}^{6}A\text{-}V = V\text{-}{}^{7}B\text{-}O + V\text{-}{}^{7}A\text{-}O, \quad (15a)$$

$$O\text{-}{}^{8}B\text{-}O + V\text{-}{}^{6}A\text{-}V = V\text{-}{}^{6}B\text{-}V + O\text{-}{}^{8}A\text{-}O, \quad (16a)$$

emphasizing that a change in the coordination of cations necessitates a redistribution of vacancies. This representation shows that the reactions can be attributed to the advantage of the association of the large cation (A) to the small anion (O) and of the small cation (B) to the large anion (V). This “small-to-large” association is thought to reduce local strain fields occurring due to the mixing of cations and anions of different sizes within the same structure. Negative signs of the enthalpy effects of reactions (15) and (16) are independently confirmed by calorimetric data [94, 100, 101]. The Part II [76] puts further constraints on the enthalpy effects of (15) and (16) through fitting them to solution calorimetry data.

An important observation, which follows from the strain driven ordering in defect fluorite, is that an event of defect formation, which causes a net change in coordination numbers, necessarily involves a large change in local strain fields. Reversely, an event of defect formation, in which the net cation coordination numbers remain the same, should cause zero or small changes in local strain fields. Below we hypothesize that the postulated ordering schemes could help in rationalizing ionic conductivity and radiation resistance data.

4.3. Constraints on coordination numbers define optimal conditions for ionic conductivity in doped zirconia.

The arguments given above suggest that the DF1 scheme dictating vacancies to avoid each other at third-nearest (and shorter) distances and to avoid direct bonding to (large) A cations represents an optimal condition for the minimization of local strain at low fractions of dopants. It follows that fluctuations in cation and anion distributions that violate these avoidance rules would tend to decay. This consideration suggests that SRO could affect mechanisms of ionic conductivity in doped zirconia. Indeed, O/V swaps that violate DF1 ordering must necessarily have low weights, while, otherwise, they would destroy the ordering. In this paragraph a possible effect of SRO on the ionic transport is discussed in a qualitative way.

O/V swaps in defect fluorite are thought to occur between edge-shared tetrahedral units in [100] direction [54]. Shimojo et al. [29] performed a molecular dynamics (MD) study of oxygen diffusion in YSZ and noted that O/V swaps predominantly occur through Zr-Zr edges of neighbouring tetrahedra, while the diffusion through Y-Y edges is effectively blocked. Krishnamurthy et al. [30] applied DFT-based molecular dynamics to compute activation barriers in YSZ for the migration through Zr-Zr, Y-Zr and Y-Y edges, constraining all other corners of two neighbouring tetrahedra to be occupied by Zr atoms. The values of 0.58, 1.29 and 1.86 eV, respectively, were obtained. These barriers were then used within a kinetic Monte Carlo (kMC) study to calculate oxygen diffusivity. Pornprasertsuk et al. [31]

computed the same barriers in YSZ with DFT taking into account different arrangements of six cations within the immediate neighbourhood of the vacancy-oxygen pair. The migration events through the Zr-Zr edge resulting in an increased number of Y cations in direct contact with the vacancy were characterized by larger activation barriers than the reverse swaps. For example, the migrations of vacancy from Zr_4V into Zr_3YO and Zr_2Y_2O clusters were characterized by larger activation energies the reverse migrations. Pietrucci et al. [32] and Kushima & Yildiz [33] further investigated the effects of vacancy-vacancy and cation-vacancy interactions. Pietrucci et al. [32] noted that a large fraction of vacancy/oxygen swaps in YSZ is forbidden due to the instability of target states, while Kushima & Yildiz [33] have found that the O/V migration events resulting in an increased number of V-V pairs at the third-nearest distance at the cost of decreasing number of 4NN pairs are associated with 0.3 – 0.8 eV higher activation barriers that the reverse transitions. Lee et al. [34, 35] applied the cluster expansion method to interpolate energies of equilibrium configurations within a cell containing 108 cations and 216 anions and combined this information with the activation energies from [30] arriving at a library of dynamic activation barriers. The kMC simulations [35] gave a remarkable agreement with experimental conductivities, significantly improving over the previous kMC studies [30, 31]. The simulations [35] correctly predicted not only the maximum in the conductivity at ~9% Y_2O_3 [102, 103], but also an increase in the activation energy with the decrease in the temperature [100]. The majority of these studies assumed the initially random cation and anion distribution. The dependence of the oxygen diffusivity on the initial distribution of Y and Zr has been specially investigated by Lee et al. [34, 35]. It has been shown that by arranging the dopant cations into rods and thus by allowing vacancies to diffuse preferably through rods of Zr_4O and Zr_4V tetrahedra, it is possible to decrease the average activation energy by 0.15-0.25 eV.

Remarkably, all studies [29-35] confirm the proposition that O/V swaps violating the DF1-type ordering are disfavoured on average by higher activation barriers. In view of these results it is logical to assume that applying the SRO of DF1-type would decrease the average activation barrier, by increasing

the fraction of O/V swaps occurring through Zr-Zr edges. The initial distribution, in which the vacancies occur exclusively within Zr_4 tetrahedra, would increase the number of swaps occurring between the symmetric local configurations Zr_4O and Zr_4V. This effect is thought to be similar to that of arranging the dopant cations into rods as done by Lee et al. [34, 35].

Thus, the plausible implication of the present study is that most of O/V swaps in DF1-type solid solution should have the activation energy of ~0.58 eV, thus differing remarkably from the experimental values of 0.8 - 1.2 eV [102-104]. In view of this prediction it is interesting to consider the recent impedance study of Ahamer et al. [104], where the experimental temperature dependence of the conductivity was accurately fitted under the assumption of two types of migration events characterized by very different values of the activation energy and very different weight factors. Importantly, the event associated with the lower value of the activation energy of 0.57 – 0.83 eV appeared to occur with a two orders of a magnitude higher frequency than the event associated with the higher value of 1.1 – 1.25 eV. We argue thus that the DF1-type ordering is very much consistent with the analysis [104] providing an explanation for the increased probability of the events characterized by low activation energies. At the same time, the rare events associated with the higher activation energy could be associated with unsuccessful attempts of vacancies to leave a domain of interconnected Zr_4-type clusters and with successful swaps allowing vacancies to diffuse into other interconnected domains. Such interconnected domains with the predominantly Zr-Zr barriers have been visualized in a recent kMC study [105].

The further implication of the present study is that the compositional dependence of the ionic conductivity must primarily result of the compositional dependence of the pre-exponential factor. Indeed, the model of Ahamer et al. [104] predicts that the conductivity at high temperatures is fully determined by the larger pool of migration events characterized by the lower value of the activation energy. This implies that the composition dependence of the relative ionic conductivity at a high temperature must be includes into the pre-exponential. Clearly, this factor should be proportional to the probability of a vacancy to remain within a DF1-type domain after a successful swap. We thus assume

the pre-exponential factor to be proportional to the probability of finding of Zr_4V (B_4V) and Zr_4O (B_4O) clusters in the immediate neighbourhood of each other. In the DF1 model ($0 \le x \le 1/3$) the tetrahedral units split into ^7B_4V, $(^8B,^8A)_4O$ and $(^7B)_2(^8B,^8A)_2O$ types. At low x values a large fraction of the latter clusters occur in the $^7B_2{}^8B_2O$ configuration. As each vacancy in DF1 is always surrounded by four B cations, the occurrence probability of ^7B_4V about a vacancy is equal to 1. The probability of finding a ^8B cation in a corner of a $(^7B)_2(^8B,^8A)_2O$ cluster is $\frac{[{}^8_{\square}B]}{[{}^8_{\square}B]+[{}^8_{\square}A]}=\frac{1-3x}{1-2x}$. Thus the probability of the joined Zr_6 cluster formed about a vacancy is $\left(\frac{1-3x}{1-2x}\right)^2$. We also assume that the pre-exponential factor is proportional to the vacancy concentration and to the probability that a vacancy swap that does not violate the vacancy-vacancy avoidance rule. To emulate a SRO distribution of anions in which vacancies do not approach each other closer than 4NN distance, we arrange vacancies over a simple cubic sublattice of the original anion lattice in which the lattice parameter is $2\boldsymbol{a}$. The first-nearest distance in this sublattice corresponds to 4NN distance in the original lattice. After a swap the vacancy finds itself between two junctions of this sublattice. Thus, a vacancy jump towards a given junction of the sublattice is allowed only when the target junction is not occupied by another vacancy. The occurrence probabilities of a vacancy and oxygen anion in junctions of the sublattice are $2x$ and $1 - 2x$, respectively. Thus, the fraction of allowed vacancy jumps is proportional to $x(1 - 2x)$ and the migration probability that contributes to the pre-exponential factor is proportional to $x(1-2x)\left(\frac{1-3x}{1-2x}\right)^2$. Fig. 8 plots this function normalized to its value at maximum. In this way the function could be compared to experimental data. The maximum is at $x \sim 0.146$. The shape of this function is in a good agreement with the data on Yb, Gd and Y-doped ZrO_2 systems, in which the maximum of conductivity occurs within the interval of 0.15-0.18 [28, 106]. Fig. 8 plots the data for A = Y, constrained by the temperature of 1273

K. The decrease of the function towards $x = 1/3$ is due to the complete extinction of $^{7}B_2{}^{8}B_2O$ clusters in DF1 model at this composition.

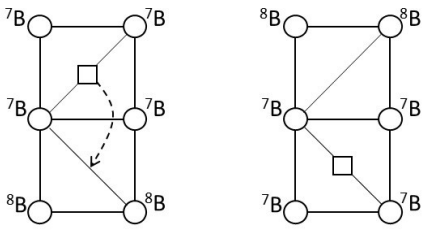

Fig. 7. Scheme of the vacancy migration mechanism in DF1-type solid solution. The squares illustrate neighbouring tetrahedral clusters.

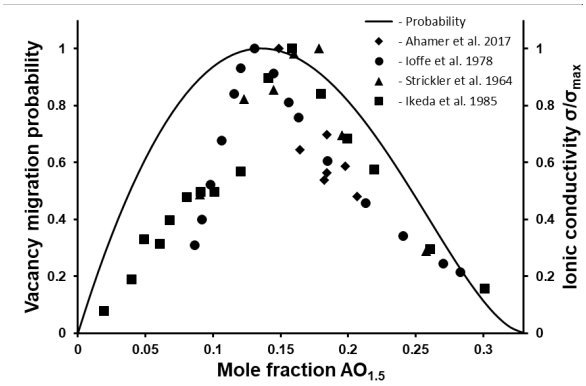

Fig. 8. Normalized migration probability of a vacancy in DF1-type solid solution. The conductivity data for YSZ ($T = 1273$ K) are taken from the sources [102-104, 107]. The break in the data at $x \sim 0.11$ - 0.13 is attributed to the tetragonal/cubic transition in YSZ [100]

The offered explanation of the occurrence of conductivity maximum in defect fluorite solid solution under the constraints of the DF1 model permits a proposition that the conductivity data for the compounds with pyrochlore $A_2B_2O_7$ composition could be also attributed to O/V swaps within a continuous network of clusters of certain same chemical type. Within such a network the O/V swaps do not cause a change in the average coordination numbers, because the initial and target states of a vacancy are similar, thus, the local strain remain nearly constant. In $Gr_xZr_{1-x}O_{2-0.5x}$ solid solution a second conductivity maximum occurs at $x \sim 0.5$. This suggests that the network that allows the continuous (zero net strain) migration is built of clusters of A_2B_2O type, where O belongs to 48f sublattice. The fraction

of such clusters is maximized in the fully ordered pyrochlore. The occurrence of the conductivity minimum at $x \sim 0.5$ in the more ordered $Nd_xZr_{1-x}O_{2-0.5x}$ system can be attributed to the lack of vacancies within the 48f network. It follows that the conductivity maximum at $x \sim 0.5$ is determined by a compromise between two contradictory conditions. The occurrence of vacancies in 48f requires a certain degree of disorder. On the other hand, this disorder tends to destroy the continuity of the network of A_2B_2 clusters. In $A_2Zr_2O_7$ systems, A={La, Nd, Sm, Eu, Gd, Y, Yb}, this compromise appears to be achieved for $Eu_2Zr_2O_7$ [11]. The break in the activation energy at $x \sim 1/3$ found in the study of van Dijk et al. [14] may mean that the barrier for the oxygen diffusion through Zr-Gd edge is reduced when the initial and target configurations of a vacancy are similar. This hypothesis seems to be confirmed by the calculations of Pornprasertsuk et al. [31] for Zr-Y system. However, the intrinsic compositional dependence of the pre-exponential factor, which has not been included in the data analysis [14], could make such a break less prominent. We suggest that conductivity data should be reanalysed assuming such a dependence. The two state model of Ahamer et al. [104] should be employed in this analysis.

The decrease in the ionic conductivity of $A_2B_2O_7$ compounds along with the P/DF transformation [11, 109, 110] can be explained by noting that in DF2-type solid solution all cations have the same 7-fold coordination. Thus, vacancy swaps could occur only between $(^7A,^7B)_4V$ and $(^7A,^7B)_4O$ clusters. Clearly, these swaps would necessarily include events, in which cations in the clusters either increase their coordination to 8, or decrease it to 6, causing fluctuations in local strain. This suggests that a continuous “zero net strain” diffusion network cannot be formed within a DF2-type fluorite.

4.4. Constraints on coordination numbers define optimal conditions for radiation resistance

The current proposition is that the radiation resistance benefits from a low rate of defect energy accumulation, while the latter is directly dependent on the defect formation energy [62]. We argue that the defect formation energy, in its turn, depends on the predominant types of cation species in a given compound. Under the assumption that the energy accumulation occurs due to cation A/B swaps, e.g. the

cation anti-site defects in pyrochlore [62], the radiation stability would be favoured by the predominance of A and B cations in the same coordination. Thus the PY/DF2 transition would be beneficial for the radiation stability, because cation swaps between ^{7}A and ^{7}B in DF2 fluorite involve no changes in coordination numbers, while such changes are inevitable due to the swaps between ^{8}A and ^{6}B in pyrochlore. Some models of radiation susceptibility suggest, however, that the radiation damage accumulates mainly due to cation Frenkel pairs [110, 111]. In the DF2 model at $x = 0.5$ both the cation sites and the cation interstitials have the same coordination of 7. On the contrary, in pyrochlore B and A sites are in 6- and 8-fold coordination, respectively, while the interstitials are 7-fold. Again, this difference suggests that the strain energy of cation Frenkel pairs would accumulate slower within the DF2-type structure than within the PY-type structure. Thus, the observed correlation between the radiation stability and the thermodynamic easiness of a P/DF transition [8, 12] may reflect the relative thermodynamic stability of DF2-like domains. The closer a given pyrochlore compound approaches the thermodynamic stability of the DF2-type structure, the larger is the volume of DF2-type domains and the higher is its radiation tolerance. Following the same idea, the ZrO_2 fluorite end-member should be characterized by another local maximum of radiation resistance as both the cation sites and the interstitials in this structure are in the same 8-fold coordination.

5. Conclusions

Application of different models of ion distribution complying with SRO allows for an accurate fit to the experimental a vs. x data for BO_2-$AO_{1.5}$ systems (B = Zr, A = {*Ln*, Y}). The main parameter in this fitting is the effective radius of the oxygen vacancy. The resulting average vacancy radius of 1.53±0.02 Å is significantly larger than the ionic radius of the oxygen anion of 1.375±0.001 Å. The conclusion of $R_V > R_O$ allows attributing the experimentally observed vacancy association to the smaller cation (Zr) to the lattice strain minimization occurring at the scale of anion-cation pairs.

The present study provides a consistent interpretation of SRO and LRO types in defect fluorite through constraints on cation coordination numbers. For example, the P/DF transformation at intermediate compositions (at the thermodynamic equilibrium) is attributed to the change from pyrochlore-type (PY) distribution based on ^{6}B and ^{8}A combination of species to DF2-type distribution based on ^{7}B and ^{7}A combination. The peculiar property of the system is that the type of SRO in the defect fluorite (in terms of the cation coordination) is inconsistent with the pyrochlore-type long-range ordering observed at low temperatures.

The developed models provide a convenient frame within which defect energies, ionic conductivity and radiation resistance data could be correlated with structural data. For example, the composition dependence of ionic conductivity in doped zirconia is attributed to composition-dependent changes in fractions of cation species, which follow from DF1-type cation and anion distribution. The proposed explanation of the composition dependence implies that the vacancy-oxygen swaps responsible for the conductivity tend to avoid local states which involve violations of vacancy-vacancy avoidance and vacancy-to-B-cation association rules. Also we argue that the stability of defect fluorite ceramics to radiation induced amorphization is likely enhanced by cation and anion distributions and compositions that are consistent with an increase in fractions of A and B cations in same coordination. For example, the DF2-type cation distribution at $x \sim 0.5$ is built of A and B cations in same 7-fold coordination. Cation A/B swaps and cation Frenkel defects in such a structure are expected to produce less structural damage. These propositions should be tested in further simulation studies. The effect of the temperature of the presently discussed ordering schemes is investigated separately in [76].

Acknowledgements

This work has been partially supported with funding from the German Federal Ministry for Education and Research (BMBF, grant 02NUK021A). Atomistic simulations were performed on RWTH and

JURECA computing clusters through the grant from the JARA-HPC awarding body. We also thank Dr. S. Finkeldei (UC Irvine) and Dr. F. Brandt (FZ-Jülich) for stimulating discussions.

Conflicts of interests

There are no conflicts to declare.

Contributions of the authors

AAB developed the main concept of constraints on cation coordination numbers in determining breaks in the variation of the lattice parameter with composition and computed key parameters of the model from a fit to experimental data. VLV further linked constrains on coordination numbers to effects of short-range and long-range order in cation and anion distribution and developed structure-property relationships. PMK performed analysis of the ab initio data for the oxygen vacancy size and provided expertise on the current research on pyrochlore-type compounds.

References

[1] H. Lehmann, D. Pitzer, G. Pracht, R. Vassen, D. Stöver, Thermal conductivity and thermal expansion coefficients of the lanthanum rare-earth-element zirconate system, J. Am. Ceram. Soc. 86 (2003) 1338-1344

[2] C.G. Levi, Emerging materials and processes for thermal barrier systems, Current Opinion in Solid State and Materials Science 8 (2004) 77-91

[3] M. N. Tsampas, F. M. Sapountzi and P. Vernoux, Applications of yttria stabilized zirconia (YSZ) in catalysis, Catal. Sci. Technol., 5 (2015) 4884-4990

[4] J.A. Kilner and R.J. Brook, A study of oxygen ion conductivity in doped non-stoichiometric oxides, Solid State Ionics 6 (1982) 237-252

[5] M. Mogensen, D. Lybye, N. Bonanos, P.V. Hendriksen, F.W. Poulsen, Factors controlling the oxide ion conductivity of fluorite and perovskite structured oxides, Solid State Ionics 174 (2004) 279-286

[6] A. J. Jacobson, Materials for Solid Oxide Fuel Cells, Chem. Mater. 22 (2010) 660-674

[7] R. Ramamoorthy, P.K. Dutta, S.A. Akbar, Oxygen sensors: Materials, methods, designs and applications, Journal of Materials Science 38 (2003) 4271-4282

[8] R.C. Ewing, W.J. Weber, and J. Lian, Nuclear waste disposal-pyrochlore ($A_2B_2O_7$): Nuclear waste form for the immobilization of plutonium and "minor" actinides, J. Appl. Phys. 95 (2004) 5949-5971

[9] G.R. Lumpkin, Ceramic waste forms for actinides, Elements 2 (2006) 365-372

[10] D. Bosbach, F. Brandt, A. Bukaemskiy, G. Deissmann, P. Kegler, M. Klinkenberg, P. M. Kowalski, G. Modolo, I. Niemeyer, S. Neumeier, V. Vinograd, Research for the Safe Management of Nuclear Waste at Forschungszentrum Jülich: Materials Chemistry and Solid Solution Aspects, Adv. Eng. Mater. (2020) 1901417, DOI: 10.1002/adem.201901417

[11] H. Yamamura H. Nishino, K. Kakinuma, K. Nomura, Electrical conductivity anomaly around fluorite-pyrochlore phase boundary, Solid State Ionics 158 (2003) 359-365

[12] S. X. Wang, B. D. Begg, L. M. Wang, R. C. Ewing, W. J. Weber, and K. V. G. Kutty, Radiation stability of gadolinium zirconate: A waste form for plutonium disposition, J. Mater. Res. 14 (1999) 4470-4473

[13] J. Lian, X. T. Zu, K. V. G. Kutty, J. Chen, L. M. Wang, and R. C. Ewing, Ion-irradiation-induced amorphization of $La_2Zr_2O_7$ pyrochlore, Phys. Rev. B 66 (2002) 054108

[14] T. van Dijk, K. J. de Vries and A. J. Burggraaf, Electrical Conductivity of Fluorite and Pyrochlore $Ln_x,Zr_{1-x},O_{2-x/2}$ (Ln = Gd, Nd) Solid Solutions, Phys. Stat. Sol. (a) 58 (1980) 115-125

[15] M. A. Subramanian, G. Aravamudan, and G. V. Subba Rao, Oxide pyrochlores – a review, Prog. Solid St. Chem. 15 (1983) 55-143

[16] K. E. Sickafus, L. Minervini, R. W. Grimes, J. A. Valdez, M. Ishimaru, F. Li, K. J. McClellan, T. Hartmann, Radiation tolerance of complex oxides, Science 289 (2000) 748-751

[17] P. K. Moon and H. L. Tuller, Ionic-conduction in the $Gd_2Ti_2O_7$- $Gd_2Zr_2O_7$ system, Solid State Ionics 28-30 (1988) 470-474

[18] H.L. Tuller, Oxygen-ion conduction and structural disorder in conductive oxides, Phys. Chem. Solids 55 (1994) 1393-1404

[19] T. Uehara, K. Koto, F. Kanamaru, and H. Horiuchi, Stability and antiphase domain structure of the pyrochlore solid solution in the ZrO_2-Gd_2O_3 system, Solid State Ionics 23 (1987) 137-143

[20] J. Wang, A Nakamura, M. Takeda, Structural properties of the fluorite- and pyrochlore-type compounds in the Gd_2O_3–ZrO_2 system $x$$GdO_{1.5}$–(1-$x$)$ZrO_2$ with $0.18 \leq x \leq 0.62$, Solid State Ionics 164 (2003) 185-191

[21] M.R. Thornber, D.J.M. Bevan, and E. Summerville, Mixed oxides of the type MO_2(fluorite)-M_2O_3. V. Phase studies in the systems ZrO_2-M_2O_3 (M = Sc, Yb, Er, Dy), J. Solid State Chem. 1 (1970) 545-553

[22] Landolt-Börnstein, Numerical Data and Functional Relationships in Science and Technology, New Series, Group 111, Crystal and Solid State Physics, Vol. 7, Crystal Structure Data of Inorganic Compounds, Part b; p. 843. Edited by K. H. Hellwege and A.M. Hellwege. Springer-Verlag, Berlin, FRG, 1975

[23] D. Steele, B.E. Fender, Structure of cubic ZrO_2-$YO_{1.5}$ solid solutions by neutron-scattering, J. Phys. C: Solid State Phys. 7 (1974) 1-11

[24] A.I. Ioffe, D.S. Ruthman, and S.V. Karpachov. On the nature of the conductivity maximum in zirconia-based solid electrolytes, Electrochim. Acta 23 (1978) 141-142

[25] W. Baukel, and R. Sheidegger, “Lattice Constants of the Cubic Solid Solution $Zr0_2$-Y_2O_3, Ber. Dtsch. Keram. Soc. 45 (1968) 610-616

[26] V.S. Stubican, R.C. Hink, and S.P. Ray, Phase-equilibria and ordering in system ZrO_2-Y_2O_3, J. Am. Ceram. Soc. 61 (1978) 17-21

[27] T. Uehara, K. Koto, Sh. Emura, and F. Kanamaru, EXAFS study of the fluorite and pyrochlore compounds in the system ZrO_2-Gd_2O_3, Solid State Ionics 23 (1987) 331-337

[28] C.R.A. Catlow, Transport in doped fluorite oxides, Solid State Ionics 12 (1984) 67-73

[29] F. Shimojo, T. Okabe, F. Tachibana, M. Kobayashi, and H. Okazaki, Molecular dynamics study of ittria stabilized zirconia. I. Structure and oxygen diffusion, J. Phys. Soc. Jpn. 61(1992) 2848

[30] R. Krishnamurthy, Y. G. Yoon, D. J. Srolovitz, and R. Car, Oxygen Diffusion in Yttria-Stabilized Zirconia: A New Simulation Model, J. Am. Ceram. Soc. 87 (2004)1821.

[31] R. Pornprasertsuk, P.Ramanarayanan, C. B.Musgrave, and F. B. Prinz, Predicting ionic conductivity of solid oxide fuel cell electrolyte from first principlesJ. Appl. Phys. 98 (2005) 103513

[32] F. Pietrucci, M. Bernasconi, A. Laio, and M. Parrinello, Vacancy-vacancy interaction and oxygen diffusion in stabilized cubic ZrO2 from first principles, Phys. Rev. B 78, (2008) 094301

[33] A. Kushima and B. Yildiz, Oxygen ion diffusivity in strained yttria stabilized zirconia: where is the fastest strain? Journal of Materials Chemistry 20 (2010). 4809

[34] E. Lee, F. B. Prinz, and W. Cai, Enhancing ionic conductivity of bulk single-crystal yttria-stabilized zirconia by tailoring dopant distribution, Phys. Rev. B, 83 (2011) 052301.

[35] E. Lee, F. B. Prinz, and W. Cai, Ab initio kinetic Monte Carlo model of ionic conduction in bulk yttria-stabilized zirconia, Modelling and Simulation in Materials Science and Engineering, 20 (2012) 065006.

[36] A. Navrotsky, P. Simoncic, H. Yokokawa, W. Q. Chen and T. Lee, Calorimetric measurements of energetics of defect interactions in fluorite oxides, Faraday Discuss. 134 (2007) 171-180

[37] P. Simoncic and A. Navrotsky, Systematics of phase transition and mixing energetics in rare earth, yttrium, and scandium stabilized zirconia and hafnia J. Am. Ceram. Soc. 90 (2007) 2143-2150

[38] T. A. Lee, A. Navrotsky, I. Molodetsky, Enthalpy of formation of cubic yttria-stabilized zirconia, J. Mater. Res. 18 (2003) 908-918

[39] A. Navrotsky, Thermodynamics of solid electrolytes and related oxide ceramics based on the fluorite structure, J. Mater. Chem. 20 (2010) 10577-10587

[40] J. Shamblin, M. Feygenson, J. Neuefeind, C. L. Tracy, F. Zhang, S. Finkeldei, D. Bosbach, H. Zhou, R. C. Ewing, and M. Lang, Probing disorder in isometric pyrochlore and related complex oxides, Nature Materials 15 (2016) 507-511

[41] S. Finkeldei, Ph. Kegler, P.M. Kowalski, C. Schreinemachers, F. Brandt, A.A. Bukaemskiy, V.L. Vinograd, G. Beridze, A. Shelyug, A. Navrotsky, and D. Bosbach, Composition dependent order-disorder transition in $Nd_xZr_{1-x}O_{2-0.5x}$

pyrochlores: A combined structural, calorimetric and ab initio modeling study, Acta Materialia 125 (2017) 166-176

[42] P.M. Kowalski, Formation enthalpy of $Ln_2B_2O_7$-type (B = Ti,Sn,Hf,Zr) compounds, Scripta Materialia 189 (2020) 7–10

[43] S. V. Ushakov, A. Navrotsky, J.A. Tangeman, K.B. Helean, Energetics of defect fluorite and pyrochlore phases in lanthanum and gadolinium hafnates, J. Am. Ceram. Soc. 90 (2007) 1171-1176

[44] M.P. Saradhi, S.V. Ushakov, A. Navrotsky, Fluorite-pyrochlore transformation in $Eu_2Zr_2O_7$ – direct calorimetric measurement of phase transition, formation and surface enthalpies, RSC Adv. 2 (2012) 3328-3334, https://doi.org/10.1039/C2RA00727D

[45] A. Bogicevic, C. Wolverton, G. Crosbie, and E. Stechel, Defect ordering in aliovalently doped cubic zirconia from first principles, Phys. Rev. B 64 (2001) 014106

[46] A. Bogicevic, and C. Wolverton, Nature and strength of defect interactions in cubic stabilized zirconia, Phys. Rev. B 67 (2003) 024106

[47] J.M. Solomon, J. Shamblin, M. Lang, A. Navrotsky, and M. Asta, Chemical ordering in substituted fluorite oxides: a computational investigation of $Ho_2Zr_2O_7$ and $RE_2Th_2O_7$ (RE=Ho, Y, Gd, Nd, La) Scientific Reports 6 (2016) 38772

[48] A. Predith, G. Ceder, C. Wolverton, K. Persson, T. Mueller, Ab initio prediction of ordered ground-state structures in ZrO_2-Y_2O_3, Phys. Rev. B 77 (2008) 144104

[49] C. Catlow, A. Chadwick, G. N. Greaves, and L. Moroney, EXAFS study of yttria-stabilized zirconia, J. Am. Ceram. Soc. 69 (1986) 272-277

[50] P. Li, I. Chen, and J. Penner-Hahn, X-ray-absorption studies of zirconia polymorphs. 2. Effect of Y_2O_3 Dopant on ZrO_2 structure, Physical Review B 48 (1993) 10074-10081

[51] P. Li, I. Chen, and J. Penner-Hahn, Effect of dopants on zirconia stabilization – an X-ray-absorption study. 1. Trivalent dopants, J. Am. Ceram. Soc. 77 (1994) 118-128

[52] K. Kawata, H. Maekawa, T. Nemoto, T. Yamamura, Local structure analysis of YSZ by Y-89 MAS-NMR, Solid State Ionics 177 (2006) 1687-1690

[53] S.T. Norberg, S. Hull, S.G. Eriksson, I. Ahmed, F. Kinyanjui, and J. J. Biendicho, Pyrochlore to Fluorite Transition: The $Y_2(Ti_{1-x}Zr_x)_2O_7$ ($0.0 \leq x \leq 1.0$) System, Chem. Mater. 24 (2012) 4294-4300

[54] M. P. van Dijk, A. J. Burggraaf, A. N. Cormack, C. R. A. Catlow, Defect structures and migration mechanisms in oxide pyrochlores, Solid State Ionics 17 (1985) 159-167

[55] P. J. Wilde and C. R. A. Catlow, Molecular dynamics study of the effect of doping and disorder on diffusion in gadolinium zirconate, Solid State Ionics 112 (3-4) (1998) 185-195, https://doi.org/10.1016/S0167-2738(97)00509-2

[56] R. E. Williford, W. J. Weber, R. Devanathan, G. D. Gale, Effects of Cation Disorder on Oxygen Vacancy Migration in $Gd_2Ti_2O_7$, J. Electroceram. 3 (1999) 409-424, DOI: https://doi.org/10.1023/A:1009978200528

[57] L. Minervini, R. W. Grimes, and K. E. Sickafus, Disorder in Pyrochlore Oxides, J. Am. Ceram. Soc. 83 (2000) 1873-1878, https://doi.org/10.1111/j.1151-2916.2000.tb01484.x

[58] M. Pirzada, R. W. Grimes, L. Minervini, J. F. Maguire, and K. E. Sickafus, Oxygen migration in $A_2B_2O_7$ pyrochlores, Solid State Ionics 140 (3-4) (2001) 201-208, https://doi.org/10.1016/S0167-2738(00)00836-5

[59] W. R. Panero, L. P. Stixrude, and R. C. Ewing, First-principles calculation of defect-formation energies in the $Y_2(Ti,Sn,Zr)_2O_7$ pyrochlore, Phys. Rev. B 70 (2004) 054110, DOI: https://doi.org/10.1103/PhysRevB.70.054110

[60] M. J. D. Rushton, R. W. Grimes, C. R. Stanek, and S. Owens, Predicted pyrochlore to fluorite disorder temperature for $A_2Zr_2O_7$ compositions, J. Mater. Res. 19 (6) (2004) 1603-1604, DOI: https://doi.org/10.1557/JMR.2004.0231

[61] M. J. D. Rushton, C. R. Stanek, A. R. Cleave, B. P. Uberuaga, K. E. Sickafus, R. W. Grimes, Simulation of defects and defect processes in fluorite and fluorite related oxides: Implications for radiation tolerance, Nucl. Instrum. Methods Phys. Res. B 255 (1) (2007) 151-157, https://doi.org/10.1016/j.nimb.2006.11.018

[62] K. E. Sickafus, R.W. Grimes, J.A. Valdez, A. Cleave, M. Tang, M. Ishimaru, S.M. Corish, C. R. Stanek and B.P. Uberuaga, Radiation-induced amorphization resistance and radiation tolerance in structurally related oxides, Nature Mater. 6 (2007) 217-223, DOI: https://doi.org/10.1038/nmat1842

[63] C. Jiang, C.R. Stanek, K.E. Sickafus, and B.P. Uberuaga, First-principles prediction of disordering tendencies in pyrochlore oxides, Phys. Rev. B 79 (2009) 104203, DOI: https://doi.org/10.1103/PhysRevB.79.104203

[64] J. Wang, F. Zhang, J. Lian, R.C. Ewing, U. Becker, Energetics and concentration of defects in $Gd_2Ti_2O_7$ and $Gd_2Zr_2O_7$ pyrochlore at high pressure, Acta Mater. 59 (2011) 1607-1618, https://doi.org/10.1016/j.actamat.2010.11.025

[65] B. P. Uberuaga, C. Jiang, K.E. Stanek K. E. Sickafus, C, Scott, R. Smith, Prediction of Irradiation Spectrum Effects in Pyrochlores, JOM 66 (12) (2014) 2578-2582, DOI: 10.1007/s11837-014-1158-x

[66] Y. Li, and P.M. Kowalski, G. Beridze, A.R. Birnie, S. Finkeldei, and D. Bosbach, Defect formation energies in $A_2B_2O_7$ pyrochlores, Scripta Materialia 107 (2015) 18-21, https://doi.org/10.1016/j.scriptamat.2015.05.010

[67] Y. Li, and P.M. Kowalski, Energetics of defects formation and oxygen migration in pyrochlore compounds from first principles calculations, J. Nucl. Mater. 505 (2018) 255-261, https://doi.org/10.1016/j.jnucmat.2017.11.005

[68] P.S. Maram, S.V. Ushakov, R.J.K. Weber, Ch.J. Benmore, and Navrotsky, Probing disorder in pyrochlore oxides using in situ synchrotron diffraction from levitated solids–A thermodynamic perspective Scientific Reports, 8 (2018) 10658, DOI: https://doi.org/10.1038/s41598-018-28877-x

[69] V. I. Aleksandrov, G. E. Valyano, B. V. Lukin, V. V. Osiko A. E. Cautbort, V. M. Tatarintsev and V. N. Filatova, Structure of single crystals of stabilized ZrO_2 (Struktura monokristallov stabilizirovannoj dvuokisi zirkonija, in Russian) lzv. Akad. Nauk SSSR, Neorg. Mater. 12 (2) (1976) 273-277

[70] R.P. Ingel and D. Lewis III, Lattice Parameters and Density for Y_2O_3-Stabilized ZrO_2, J. Am. Ceram. Soc. 69 (4) (1986) 325-332, https://doi.org/10.1111/j.1151-2916.1986.tb04741.x

[71] V.B. Glushkova, F. Hanic, and L.V. Sazonova, Lattice parameters of cubic solid solution in the systems u R_2O_3-(1-u) MO_2, Ceram. Int. 4 (4) (1978) 176-178

[72] M. Yashima, N. Ishizawa, M. Yoshimura, Application of an Ion-Packing Model Based on Defect Clusters to Zirconia Solid Solutions: I, Modeling and Local Structure of Solid Solutions, J. Am. Ceram. Soc. 75(6) (1992) 1541-1549, https://doi.org/10.1111/j.1151-2916.1992.tb04222.x

[73] M. Yashima, N. Ishizawa, M. Yoshimura, Application of an Ion-Packing Model Based on Defect Clusters to Zirconia Solid Solutions: II, Applicability of Vegard's Law, J. Am. Ceram. Soc. 75 (6) (1992) 1550-1557, https://doi.org/10.1111/j.1151-2916.1992.tb04223.x

[74] D-J. Kim, Lattice Parameters, Ionic Conductivities, and Solubility Limits in Fluorite-Structure MO_2 Oxide [M = Hf^{4+}, Zr^{4+}, Ce^{4+}, Th^{4+}, U^{4+}] Solid Solutions, J. Am. Ceram. Soc. 72 (8) (1989) 1415-1421, https://doi.org/10.1111/j.1151-2916.1989.tb07663.x

[75] S. J. Hong and A. V. Virkar, Lattice Parameters and Densities of Rare-Earth Oxide Doped Ceria Electrolytes, J. Am. Ceram. Soc. 78 (2) (1995) 433-439, https://doi.org/10.1111/j.1151-2916.1995.tb08820.x

[76] V.L. Vinograd and A.A. Bukaemskiy. Acta Materialia (subm)

[77] V.I. Strakhov, J.V. Klucharov, G.G. Sergeev, Interaction of ZrO_2 and Nd_2O_3 during isothermal treatment (Vzaimodejstvie ZrO_2 in Nd_2O_3 v uslovijah izotermocheskoj obrabotki, in Russian), Zh. Prikl. Khim. 49 (1973) 2083-2085

[78] C. Wang. Experimental and computational phase studies of ZrO_2-based systems for thermal barrier coatings. PhD Thesis, Stuttgart, 2006

[79] K. Shinozaki, H.R. Sun, K. Uematsu, N. Mizutani, and M. Kato, Sintering of Sm_2O_3-ZrO_2 Solid Solution, Nippon Kagaku Kaishi 9 (1981) 1454-1461, https://doi.org/10.1246/nikkashi.1981.1454

[80] W. K. Chang, A. A. Wang, and Y. H. Lee, Oxygen-induced structural change of zirconia by adding rare earth oxides with solid state method, J. Alloy Comp. 249 (1997) 251-255, https://doi.org/10.1016/S0925-8388(96)02739-9

[81] Y. Tabira, R. L. Withers, Structure and Crystal Chemistry as a Function of Composition across the Wide Range Nonstoichiometric $(1-\varepsilon)ZrO_2 \cdot \varepsilon SmO_{1.5}$, $0.38<\varepsilon<0.55$, Oxide Pyrochlore System, J. Solid State Chem. 148 (1999) 205-214, https://doi.org/10.1006/jssc.1999.8433

[82] A. Nakamura, N. Masaki, H. Otobe, Y. Hinatsu, J. Wang, M. Takeda, Defect-fluorite oxides $M_{1-y}Ln_yO_{2-y/2}$(Ln = lanthanide; M = Hf, Zr, Ce, U, Th): Structure, property, and applications, Pure Appl. Chem. 79 (2007) 1691-1729, http://dx.doi.org/10.1351/pac200779101691

[83] M. Perez, Y. Jorba, Zirconia-Rare Earth Oxide system, Ann. Chim. 7 (1962) 479

[84] A. Nakamura, New defect-crystal-chemical approach to non-Vegardianity and complex defect structure of fluorite-based MO_2–$LnO_{1.5}$ solid solutions (M^{4+} = Ce, Th; Ln^{3+} = lanthanide) part I: Model description and lattice-parameter data analysis, Solid State Ionics 181 (2010) 1543-1564, https://doi.org/10.1016/j.ssi.2010.09.019

[85] A. Nakamura, New defect-crystal-chemical approach to non-Vegardianity and complex defect structure of fluorite-based MO_2–$LnO_{1.5}$ solid solutions (M^{4+} = Ce, Th; Ln^{3+} = lanthanide): Part II:

Detailed local-structure and ionic-conductivity analysis, Solid State Ionics 181 (2010) 1631-1653, https://doi.org/10.1016/j.ssi.2010.09.022.

[86] R.D. Shannon, Revised effective ionic radii and systematic studies of interatomic distances in halides and chalcogenides, Acta Crystallogr. A 32 (5), (1976) 751-767, https://doi.org/10.1107/S0567739476001551.

[87] D. Marrocchelli, S.R. Bishop, H.L. Tuller, and B. Yildiz, Understanding Chemical Expansion in Non-Stoichiometric Oxides: Ceria and Zirconia Case Studies, Adv. Funct. Mater. 22 (9) (2012) 1958-1965, https://doi.org/10.1002/adfm.201102648

[88] D. Marrocchelli, S.R. Bishop, J. Kilner, Chemical expansion and its dependence on the host cation radius, J. Mater. Chem. A 1 (2013) 7673-7680, https://doi.org/10.1039/C3TA11020F

[89] P. Giannozzi, et al., QUANTUM ESPRESSO: a modular and open-source software project for quantum simulations of materials, J. Phys.: Condens. Matter 21 (2009) 395502, doi:10.1088/0953-8984/21/39/395502

[90] D. Vanderbilt, Soft self-consistent pseudopotentials in a generalized eigenvalue formalism, Phys. Rev. B 41 (1990) 7892, DOI: https://doi.org/10.1103/PhysRevB.41.7892

[91] J. P. Perdew, K. Burke, M. Ernzerhof, Generalized Gradient Approximation Made Simple, Phys. Rev. Lett. 77 (1996) 3865, DOI: https://doi.org/10.1103/PhysRevLett.77.3865

[92] R.D. Shannon, and C.T. Prewitt, Effective ionic radii in oxides and fluorides, Acta Crystallogr. B 25 (1969) 925-946, doi:10.1107/S0567740869003220

[93] S. M. Koohpayeh, J. J. Wen, B. A. Trump, C. L. Broholm, and T. M. McQueen, Synthesis, floating zone crystal growth and characterization of the quantum spin ice $Pr_2Zr_2O_7$ pyrochlore, J. Crystal Growth 402 (2014) 291-298 https://doi.org/10.1016/j.jcrysgro.2014.06.037

[94] A. V. Radha, S. V. Ushakov and A. Navrotsky, Thermochemistry of lanthanum zirconate pyrochlore, J. Mater. Res. 24 (2009) 3350-3357, DOI: https://doi.org/10.1557/jmr.2009.0401

[95] J. P. Perdew, A. Ruzsinszky, G. I. Csonka, O. A. Vydrov, G. E. Scuseria, L. A. Constantin, X.L. Zhou, K. Burke, Restoring the Density-Gradient Expansion for Exchange in Solids and Surfaces, Phys. Rev. Lett. 100 (2008) 136406, DOI:https://doi.org/10.1103/PhysRevLett.100.136406

[96] K. R. Whittle, L. M. D. Cranswick, S.A.T. Redfern, I.P. Swainson, G.R. Lumpkin, Lanthanum pyrochlores and the effect of yttrium addition in the systems $La_{2-x}Y_xZr_2O_7$ and $La_{2-x}Y_xHf_2O_7$, J. Solid State Chem. 182 (2009) 442-450 https://doi.org/10.1016/j.jssc.2008.11.008

[97] R. Clements, J. R. Hester, B. J. Kennedy, C.D. Ling, A.P.J. Stampfl, The fluorite–pyrochlore transformation of $Ho_{2-y}Nd_yZr_2O_7$, J. Solid State Chem. 184 (2011) 2108-2113, https://doi.org/10.1016/j.jssc.2011.05.054

[98] G. Stapper, M. Bernasconi, N. Nicoloso, and M. Parrinello, Ab initio study of structural and electronic properties of yttria-stabilized cubic zirconia, Phys. Rev. B 59 (1999) 797

[99] F. Pietrucci, M. Bernasconi, C. Di Valentin, F. Mauri, and C. J. Pickard, EPR *g*-tensor of paramagnetic centers in yttria-stabilized zirconia from first-principles calculations, Phys. Rev. B 73 (2006) 134112

[100] A. Navrotsky, S. Ushakov Thermodynamics of Oxide Systems Relevant to Alternative Gate Dielectrics in A. A. Demkov and A. Navrotsky eds. Materials Fundamentals of Gate Dielectrics 2005, Chapter 3, page 73

[101] M.P. Saradhi, S.V. Ushakov, A. Navrotsky, Fluorite-pyrochlore transformation in $Eu_2Zr_2O_7$ – direct calorimetric measurement of phase transition, formation and surface enthalpies, RSC Adv. 2 (2012) 3328-3334, https://doi.org/10.1039/C2RA00727D

[102] A. I. Ioffe, D. S. Rutman, S. V. Karpachov, On the nature of the conductivity maximum in zirconia-based solid electrolytes, Electrochim. Acta 23 (1978) 141-142.

[103] S. Ikeda, O. Sakurai, K. Uematsu, N. Mizutani, M. Kato, Electrical conductivity of yttria-stabilized zirconia single crystals, J. of Materials Science 20 (1985) 4593-4600

[104] C. Ahamer, A.K. Opitz, G.M. Rupp, and J. Fleig, Revisiting the Temperature Dependent Ionic Conductivity of Yttria Stabilized Zirconia (YSZ), J. Electrochem. Soc. 164 (2017) F790-F803

[105] M. Jaipal and A. Chatterjee, Mesoscale understanding of ionic conduction in yttria stabilized zirconia: the nanoscale percolation network and its effect on O^{2-} ion movement, Modelling Simul. Mater. Sci. Eng. 27 (2019) 064003

[106] J.A. Kilner and B.C.H. Steele, in: Non-stoichiometric oxides, ed. O.T. Sorensen (Academic Press, New York, 1981).

[107] D. W. Strickler, W. G. Carlson, Ionic conductivity of cubic solid solutions in the system CaO-Y_2O_3-ZrO_2, J. Am. Ceram. Soc. 47, 3 (1964) 122-127.

[108] M.P. van Dijk, K.J. de Vries, A.J. Burggraaf, Oxygen ion and mixed conductivity in compounds with the fluorite and pyrochlore structure, Solid State Ion. 9-10 (1983) 913-919, https://doi.org/10.1016/0167-2738(83)90110-8.

[109] J.A. Díaz-Guillén, A.F. Fuentes, M.R. Díaz-Guillén, J.M. Almanza, J. Santamaría and C. León, The effect of homovalent A-site substitutions on the ionic conductivity of pyrochlore-type $Gd_2Zr_2O_7$, J. Power Sources, 186 (2) (2009) 349-352

[110] R. Devanathan, W. J. Weber and J. D. Gale, Radiation tolerance of ceramics—insights from atomistic simulation of damage accumulation in pyrochlores, Energy Environ. Sci. 3 (2010) 1551-1559, DOI: 10.1039/c0ee00066c

[111] A. Chartier, G. Catillon and J.-P. Crocombette, Key Role of the Cation Interstitial Structure in the Radiation Resistance of Pyrochlores, Phys. Rev. Lett. 102 (15), (2009) 155503, DOI: https://doi.org/10.1103/PhysRevLett.102.155503